18

Nanowire Formation under Femtosecond Laser Radiation in Liquid

Yasuhiko Shimotsuma, Kiyotaka Miura and Kazuyuki Hirao
Kyoto University,
Japan

1. Introduction

The size and shape of nanoscale materials provide excellent control over many of the physical and chemical properties, including electrical and thermal conductivity, magnetic properties, luminescence, and catalytic activity (Lieber, 1998). In particular, the synthesis and morphological control of nanosized particles, which exhibit surprising and novel phenomena based on the unique property called the quantum size effect, are attractive to chemists and physicists (Alivisatos, 1996). In recent years, nanoparticles are widely used in many applications ranging from biosensing (Anker et al., 2008; Elghanian et al., 1997; Lin et al., 2006), plasmonic devices (Ferry et al., 2008; Maier et al., 2003), and multifunctional catalysts (Hu et al., 1999; Lu et al., 2004). There are a wide variety of techniques that are capable of creating nanoparticles with various morphology and production yield. These nanoparticle formation approaches are typically grouped into two categories: 'top-down' and 'bottom-up'. The first involves the breaking down of large pieces of bulk material into the required nanostructures. The second involves the building of nanostructures, atom-by-atom or molecule-by-molecule in a gas phase or solution. These two approaches have evolved separately and reached the limits in terms of feature size and quality, in recent years, leading to exploring novel hybrid approaches in combining the top-down and bottom-up methods. Colloidal chemists have gained excellent controlled nanosized particles for several spherical metal and semiconductor compositions, which has led to the discovery of quantum size effect in colloidal nanocrystals (Alivisatos, 1996). However, various bottom-up approaches for making morphologically controlled nanoparticles have been found; most of these solution methods are based on thermal process. On the other hand, top-down approaches have been developed for producing metal and semiconductor nanowires, nanobelts, and nanoprisms (Hu et al., 1999; Pan et al., 2001; Jin et al., 2001). In particular, the laser-induced ablation method has become an increasingly popular approach for making nanoparticles due to the applicability to various target materials in an ambient atmosphere (Jia et al., 2006a; Kawasaki & Masuda, 2005; Link et al., 1999; Sylvestre et al., 2004; Tamaki et al., 2002; Tull et al., 2006). Recently, various shape-controlled nanoparticles, such as nanowires (Morales & Lieber, 2008), nanotubes (Rao et al., 1997), and composite nanostructures (Zhang et al., 1998), have been fabricated by this technique. More recently, pulsed laser ablation in liquid has become profoundly intrigued for preparing nanoparticles from the viewpoint of the concise procedure and the ease of handling (Kawasaki & Masuda, 2005; Tamaki et al., 2002; Shimotsuma et al., 2007).

Besides, in recent decades, increasing interest has focused on the femtosecond laser field due to its unique characteristics based on the nonlinear optical effects deriving from ultrashort pulse width and high peak power density (Cavanagh et al., 1993; Stuart et al., 1995). Especially, by connecting the femtosecond laser technology with nanotechnology, an effective approach was provided to prepare and modify nanostructures in micro devices (Kabashin et al., 2003; Kanehira et al., 2005; ; Link et al., 2000; Muskens et al., 2006; Qiu et al., 2004; Shimotsuma et al., 2003, 2007). For example, the ripple nanostructures, which are aligned along the femtosecond laser polarization direction, have been observed on the surface of the metal and semiconductor caused by the interferences between the scattering incident femtosecond laser field and the surface plasmon-polariton waves (Jia et al., 2006a). We have recently reported the first experimental evidence of the periodic nanostructures embedded in silica glass after irradiation by a single focused beam of a femtosecond laser (Shimotsuma et al., 2003). This phenomenon can be interpreted in terms of interference between the incident laser light field and the generated bulk electron plasma waves, resulting in the periodic modulation of electron plasma concentration and the structural changes in transparent material. A great success has been achieved in forming zero dimensional nanoparticles by using intense ultrashort light pulses radiation. We have successfully fabricated a colourful micro-pattern composed of Au or Ag nanoparticles inside a glass matrix (Qiu et al., 2004; Shimotsuma et al., 2007). Podlipensky and co-workers reported the formation of anisotropic Ag nanoparticles in glass which were elongated in the direction parallel to the femtosecond laser polarization (Podlipensky et al., 2003). Link and co-workers reported the size and shape change of Au nanorods under both femtosecond and nanosecond laser irradiation in solution (Link et al., 1999). The limited prior exploration for preparing one-dimensional nanoparticles by a femtosecond laser was concentrated on their fabrication on the materials' surface. Jia et al. reported ZnSe nanowires' growth induced by the femtosecond laser. Yet the nanowires grew only on the ablation crater located on the surface of ZnSe wafer (Jia et al., 2006b). Mazur et al. reported the production of submicrometer-sized spikes that consisted of the silicon on the silicon wafer after irradiating a silicon surface with a femtosecond laser (Baldacchini et al., 2006; Shen et al., 2004). Thus it should be interesting to investigate the preparation and evolution of nanowires under intense ultrashort light fields, which might reveal the interaction between the photons and the excited plasmons (materials) in the nanoscale.

In this Chapter, we present formation of one-dimensional metal Cu (Nakao et al., 2008; Shimotsuma et al., 2007) and ZnO (Lee et al., 2008, 2009) nanoparticles under femtosecond laser irradiation in liquid. It should be interesting to investigate the preparation and evolution of nanowires under intense ultrashort light fields, which reveals that the growth mechanism of Cu and ZnO nanowires could be a nucleation growth process (Chang et al., 2008; Wu et al., 2010).

2. Photofragmentation and evolution of metal Cu nanowire

In this section, the photofragmentation from Cu micro-flakes to nanowires and nanospheres via femtosecond laser radiation in alcohol solution was described. This phenomenon has provided the two distinct surface plasmon resonances based on the characteristic shape. The observed Cu nanowires of 50 nm diameter could be fragmented from the initial flakes as a result of the interference between the light field and the surface plasmon wave. By observing the morphology transformation of nanowires with time, the mechanism of Cu

nanowires growth with femtosecond laser irradiation in the solution was also presented. Interestingly, the growth of the Cu nanowires was influenced by the incident light polarization. Other starting materials, e.g. Cu microspheres, were also tested to fabricate nanowires under the same technique to verify the mechanism and procedure of nanowires' growth by another process. Furthermore, we demonstrate that the morphological control of Cu nanoparticles, dispersed in various alcohol solutions, under femtosecond laser irradiation. Beyond the basic understanding, such Cu nanowires have possible applications in the areas of plasmonic devices (Liu et al., 2008), surface-enhanced Raman scattering (SERS) (Sauer et al., 2006), and medicinal imaging (Desvaux et al., 2005).

2.1 Photo-conversion of Cu micro-flakes to nanowires

We used commercially available Cu micro-flakes produced by a chemical reduction method, which were 5 μm in size and 100 nm thick. A small amount of the Cu flakes, 0.36 mg, was mixed with 4.5 mL of 99.5% alcohol solution in a rectangular quartz vessel of $1 \times 1 \times 5$ cm^3 with a vessel thickness of 1.25 mm. The laser radiation in Gaussian mode produced by a regenerative amplified mode-locked Ti:sapphire laser (Coherent Inc., 100 fs pulse duration, 1 kHz repetition rate) operating at a wavelength of 800 nm was focused via a microscope objective (Nikon; LU Plan Fluor, 20× 0.40 N.A.) into the alcohol-suspended Cu micro-flakes placed on a magnetic stirrer. The typical beam waist diameter and laser energy fluence were estimated at ~ 4 μm and 2.4×10^3 J/cm^2, respectively. The polarization of the laser light was set linear or circular by a half-wave or a quarter-wave plate placed in the incident beam before the focusing optics. A schematic of the experimental setup is shown in Fig. 1. Before

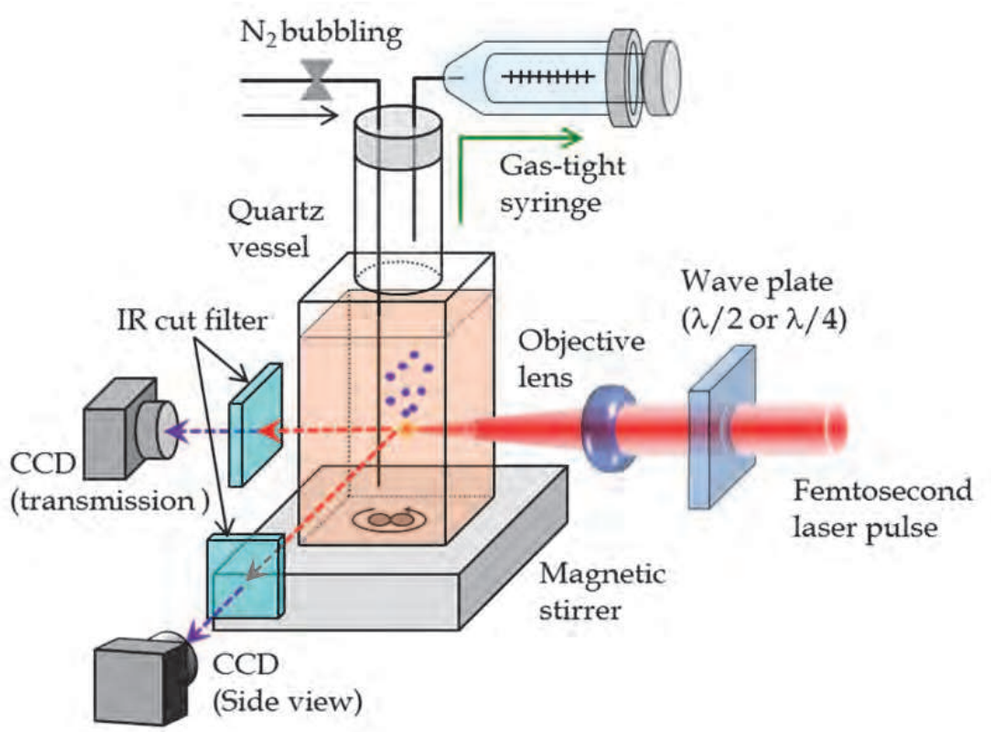

Fig. 1. Schematic of an experimental setup including gas trapping system during femtosecond laser pulse irradiation.

laser irradiation, the suspension was deaerated by bubbling nitrogen gas into it for 15 minutes. To keep as many Cu micro-flakes as possible suspended in the solution, the solution was continuously stirred with a magnetic stirrer during laser irradiation. The generated gas during laser irradiation was trapped in a gas-tight syringe at atmosphericpressure, and then analyzed by a gas chromatography (Shimadzu Corp., GC-2014). After laser irradiation, absorption spectra of the Cu suspension were measured by a spectrophotometer (JASCO, V-570). In order to analyze the nucleation site just after femtosecond laser irradiation, the suspension was immediately dropped onto a silicon substrate and the solvent was evaporated at room temperature. To reveal the growth mechanism of Cu particles, after laser irradiation, the suspensions were left at rest in a temperature-controlled bath having a constant temperature of 40 or 60 °C. The Cu particles after femtosecond laser irradiation were characterized by a field-emission scanning electron microscopy (JEOL, JSM-6700F), a transmission electron microscope (JEOL, JEM-2010F), and a field-emission electron probe micro analyzer (JEOL, JXA-8500F). All of the experiments were carried out at ambient temperature and pressure.

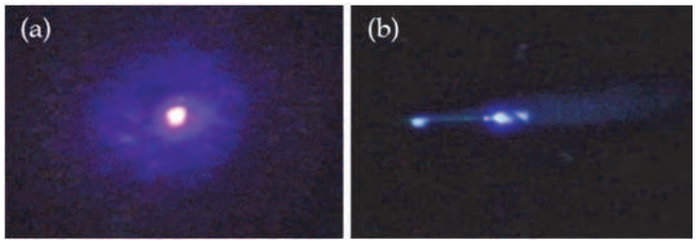

Fig. 2. CCD images of the focal spot during femtosecond laser irradiation into alcohol solution (methanol) along (a) and perpendicular (b) to the laser axis.

We observed the focal spot during femtosecond laser irradiation into alcohol solution along and perpendicular to the laser axis by using CCD camera (Fig. 2). These photos clearly indicate the generation of white-light filaments. It is well known that when a high intense femtosecond laser pulse is launched in gases (Braun et al., 1995; Corkum et al., 1986), liquids (Liu et al., 2002), and solids (Tzortzakis et al., 2001), it self-focuses and self-transforms into a white-light emission during femtosecond laser filamentation. Filamentation is commonly explained in terms of a balance between two nonlinear effects: Kerr self-focusing inducing a change of the refractive index of the medium proportional to the laser intensity; plasma defocusing through multiphoton and/or tunnel ionization of the medium in the high-intensity zone.

The pulse width at the focus after propagating in the dispersion medium can be estimated by the following equation:

$$\Delta\tau_{out} = \sqrt{\Delta\tau_{in}^2 + \frac{4(\ln 2)^2 \lambda^6 L^2}{\pi^2 c^4 \Delta\tau_{in}^2}\left(\frac{d^2 n}{d\lambda^2}\right)} \tag{1}$$

where $\Delta\tau_{in}$, $\Delta\tau_{out}$, λ, L, c, $d^2n/d\lambda^2$ are the input pulse width, the output pulse width, the wavelength, the propagation length in dispersion medium, the speed of light, and the second derivative of refractive index with respect to wavelength, respectively. From this equation, the input laser pulse width of 100 fs was stretched to 110 fs after propagating

through 10 mm in methanol (Fig. 3). Such elongation of pulse width in alcohol solution does not make any difference in nonlinear light-matter interaction.

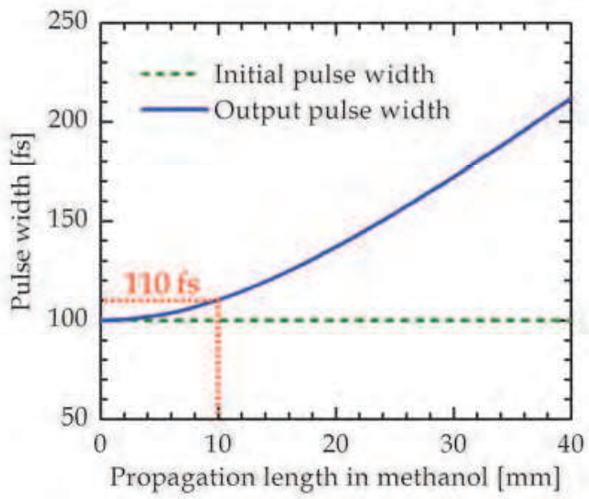

Fig. 3. Output pulse width after propagating in dispersion medium (methanol solution).

Fig.4 (a) shows the sequence of absorption spectra of the suspension, taken as a function of laser irradiation time. Minor absorption was observed for the dilute suspension of Cu micro-flakes in the wavelength region from 330 to 800 nm before the femtosecond laser irradiation while there were two apparent surface plasmon peaks in the absorbance (λ_{abs} = 380 nm and 600 nm) during laser irradiation. The fluctuation of the surface plasmon peaks are considerably weaker as compared to the background interband transition that predominates

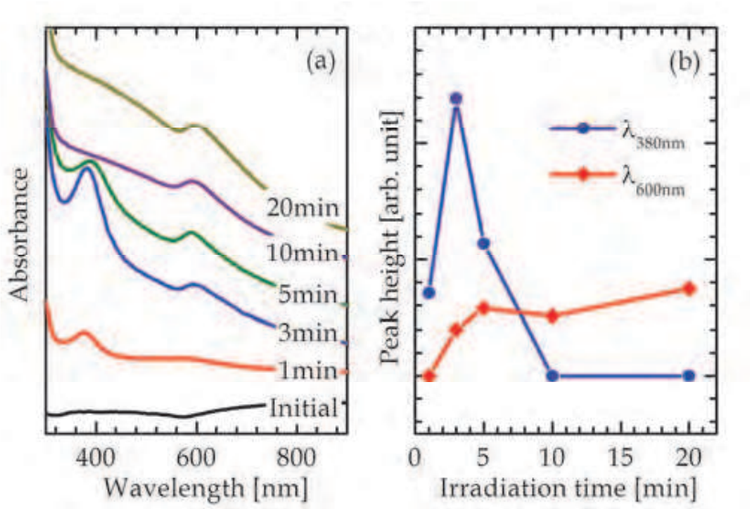

Fig. 4. (a) Sequence absorption spectra taken as a function of laser irradiation time at a pulse energy fluence of 3.5×10^3 J/cm^2. Each curve is shifted with respect to the next longer irradiation time. (b) Peak height profiles of the corresponding absorption at λ = 380 nm and 600 nm as a function of laser irradiation time.

the high-energy wing (λ < 320 nm) of the spectra (Kawasaki & Masuda, 2005). We also observed an increase in intensity of the surface plasmon absorption for the spherical particles at λ_{abs} = 600 nm with a concomitant growth of a new peak at λ_{abs} = 380 nm (Fig.4 (b)). Indeed, the surface plasmon absorption of 10 nm spherical Cu nanoparticles is located at 560 nm, which can be predicted by Mie theory with no free electron density correction (Lipinska-Kalita et al., 2005). After 10 min, the peak at 380 nm completely disappeared. In the case of long pulse laser irradiation, these unexplained peaks have not been observed (Kawasaki & Masuda, 2005).

Scanning electron images (SEIs), when correlated with the time-dependent absorption spectroscopic observations, show that the initial Cu micro-flakes (size: ~ 5 μm, thick: ~ 0.1 μm) were converted to nanowires after the femtosecond laser irradiation between 1 and 5 minutes (Fig.5 (a) ~ (d)). During initial stages of the nanowires formation, both micro-flakes and nanowires can be seen (Fig. 5 (b)). The diameter of the nanowire increases with laser-irradiation time. The growth rate of the diameter of nanowires increases with the pulse repetition rate from 10.2 to 54.2 nm/min (Fig. 6 (a)). After 10 minutes irradiation, nearly all of the nanowires are converted to the nanospheres of 10 ~ 70 nm diameter (Fig. 5 (e), (f)). Detailed FE-SEM observations revealed that the diameters of Cu nanowire were about 62, 159, 270 nm for the number of light pulses of 6×10^4, 180×10^4, 300×10^4, respectively, and for the pulse energy of 0.4 mJ, corresponding to intensity of 1.6×10^{16} W/cm^2. This indicated a linear dependence of the nanowire diameter on the number of light pulses (Fig. 6 (c)). During the nanowire growth stage, the lengths of nanowires slightly increased from 3 μm and eventually were saturated to 6 μm (Fig. 6 (b)). The extremely small Cu clusters could be also generated by the fragmentation of a portion of nanowire and consumed in this nanowire growth. Finally, nanospheres of 10 ~ 70 nm were formed by the fragmentation of nanowires along with the termination in growth of the nanowires. The Cu clusters were also formed from either fragmentation or dissolution of the nanospheres. The nanowires act as the sources of nanospheres and clusters. These data clearly show that the Cu nanospheres are dissociated from the initial flakes via

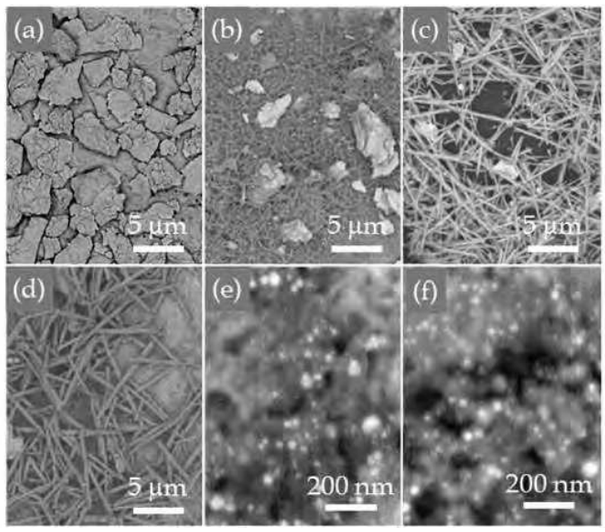

Fig. 5. SEIs indicating the morphology changes (a) before irradiation and after (b) 1, (c) 3, (d) 5, (e) 10, and (f) 20 minutes of the femtosecond laser irradiation.

nanowires formation. This photo-conversion is also indicated in the absorption spectral changes. Namely, the absorption peaking at λ_{abs} = 380 nm could be assigned to the transverse surface plasmon resonance of Cu nanowires.

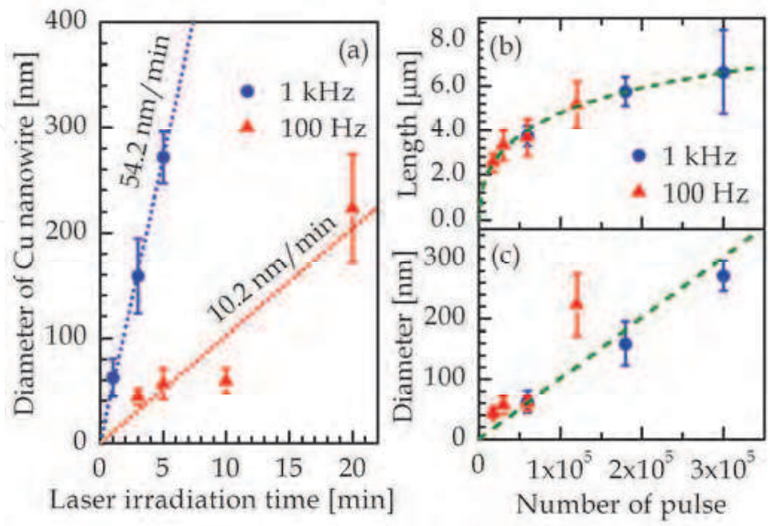

Fig. 6. (a) Diameter of the Cu nanowire as a function of laser irradiation time. (b) Length and (c) diameter of the Cu nanowire as a function of irradiated number of pulse with intensity of 1.6×10^{16} W/cm^2.

To understand the mechanism of one-dimensional Cu nanoparticles under the intense ultrashort light pulses and to compare the results from different starting materials, other starting materials, e.g. Cu microspheres and Cu sheet, were also tested to fabricate nanowires and nanorods under the same experimental procedure (Fig. 7). A similar structural evolution process was found for the microspheres (Fig. 7 (a)), which was also firstly formation of the short nanorods on the surface of microspheres (Fig. 7 (b)), then the.

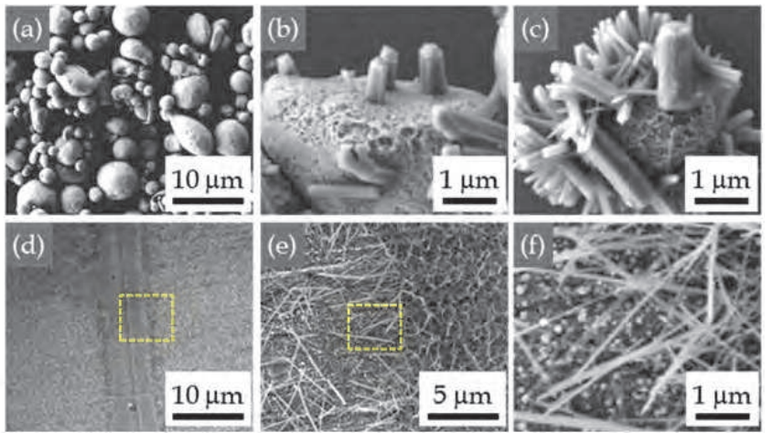

Fig. 7. SEIs of Cu microspheres before laser irradiation (a) and nanorods prepared with the different irradiation time: (b) 10 min and (c) 20 min. (d) SEI of Cu sheet after femtosecond laser scanning. The images in (e) and (f) are the high magnified images of the dotted regions in (d) and (e), respectively.

amount and length of the nanorods increased at the cost of the microspheres and finally the microspheres were reduced in size to the nanospheres with increasing laser irradiation time, as shown in Fig. 7 (c). This means that the nucleation growth mechanism of nanoparticles is the same with another materials evolving in the condition of intense ultrashort light pulses. This process could find wide applications for the preparation of one-dimensional nanoparticles. Indeed, we have also observed the growth of nanowire on the surface of Cu sheet after femtosecond laser irradiation (Fig. 7 (d) ~ (f)). Compared with the typical formation of Cu nanowires of 85 nm diameter from micro-flakes, it was nanorods with the average length and diameter of 1 μm and 280 nm, respectively that formed in the methanol solution. In addition, it seemed that a slightly longer irradiation time (20 min) was needed for the transformation to the nanorods, indicating that higher laser energy was involved in the change to the nanorods from microspheres than that in the conversion from the micro-flakes to nanowires

2.2 Characterization of Cu nanowires

Fig. 8 (b), (c) show the typical SEIs of Cu nanowires, which were synthesized by femtosecond laser with an irradiation time of 5 min. It was clearly demonstrated that nanowires, with an average length of 1.0 μm and an average diameter of 85 nm were formed via simple femtosecond laser irradiation. Comparing with the original Cu micro-flakes, shown in Fig. 8 (a), it is clear that almost all of micro-flakes transferred to the nanowire structure in the methanol after 5 min irradiation, indicating that femtosecond laser irradiation provided a highly effective way for the nanowires formation. Some small nanospheres attached to the edge of nanowires (Fig. 8 (c)) were thought to contribute to the growth of nanowires. Interestingly, many clumps consisting of needle-like nanowires along all directions were found in the images, which implied that one nucleation site was located in the centre and grew up to form the nanowires.

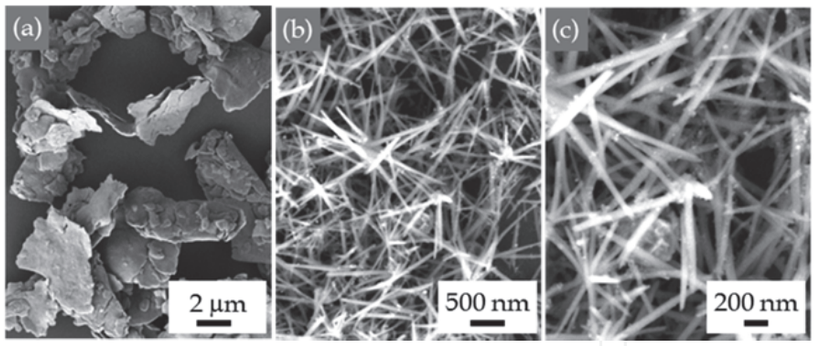

Fig. 8. Typical SEIs of Cu micro-flakes before femtosecond laser irradiation (a) and Cu nanowires observed after 5 min femtosecond laser irradiation. The images are shown in two different scales: (b) low- and (c) high-magnification image for the same area.

A detailed TEM analysis of Cu nanowires and nanospheres prepared in ethanol has been performed. Fig. 9 shows TEM observations of Cu nanowires after femtosecond laser irradiation for 3 minutes. Schematic diagrams of the analysis methods are also shown. The conventional observations indicate that the nanowires' surfaces are composed of polycrystalline Cu_2O (Fig. 9 (a), (b), (e)). Furthermore, the cross-sectional observations clearly demonstrate that nanowires are partially oxidized from the surface to a depth of

about 5 nm (Fig. 9 (d)). On the other hand, the inner part of the nanowires was composed of polycrystalline metallic Cu (Fig. 9 (c), (d), (f)). Indeed, the electron diffraction patterns of the inner and surface parts indicate that the observed areas were composed of metallic Cu (Fig. 9 (e)) and Cu_2O (Fig. 9 (f)), respectively.

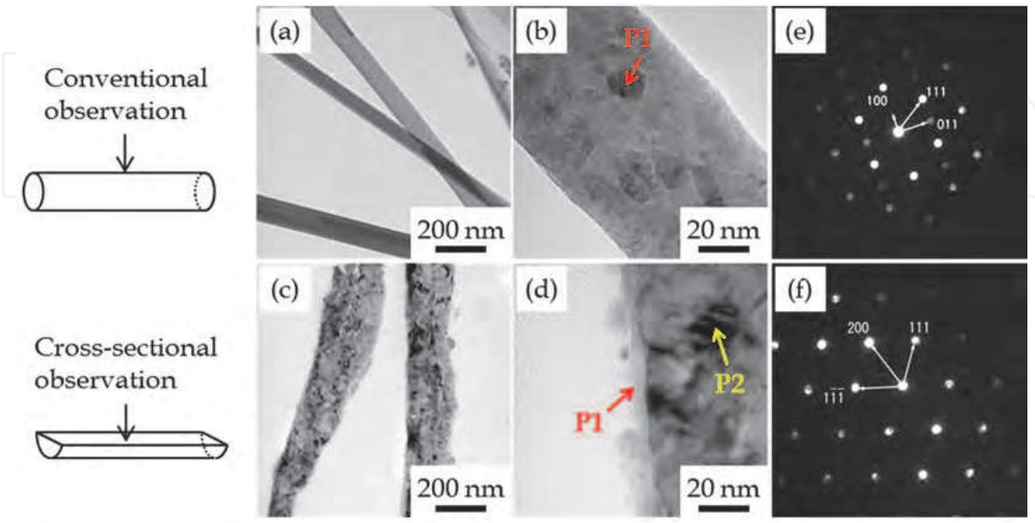

Fig. 9. TEM observations of Cu nanowires after femtosecond laser irradiation for 3 minutes. Schematic diagrams of the analysis methods are also shown on the left hand side. Two types of observations were carried out: conventional (a), (b) and cross-sectional (c), (d). The images are shown at two different scales: low magnification images (a), (c) and high magnification images (b), (d) for the same area. Arrows P1 and P2 in (d) show the analysis points of the electron diffraction patterns. The electron diffraction patterns at P1 and P2 are shown in (e) and (f), respectively.

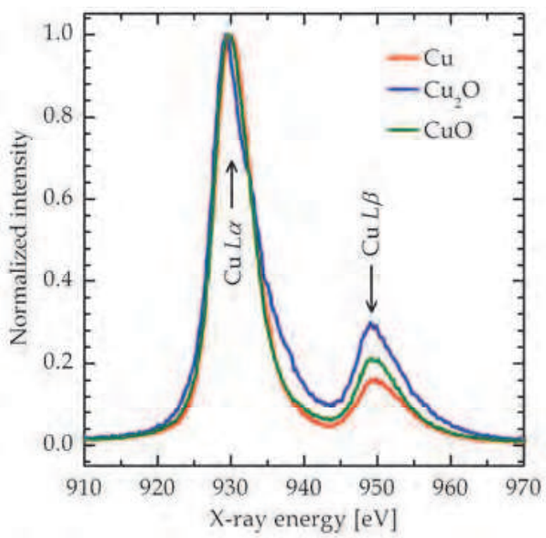

Fig. 10. Typical Cu $L\alpha$ and $L\beta$ X-ray fluorescence spectra of various copper oxide compounds.

In order to reveal the chemical state inside Cu nanowires, we carried out chemical state mapping of Cu on the cross-sectional surface by using a field-emission electron probe micro-analyzer (JEOL, JXA-8500F). The chemical state of copper by using EPMA can be determined from the difference in the peak intensity ratio of $I_{L\alpha}/I_{L\beta}$ X-ray fluorescence spectra of Cu (Kawai et al., 1993). Typical X-ray fluorescence spectra of various copper oxide compounds and the peak intensity ratio of $I_{L\alpha}/I_{L\beta}$ were shown in Fig. 10 and Table 1, respectively. Based on these relationships, we converted the spectral mapping into the chemical state mapping (Fig. 11). These observations revealed that the main chemical composition inside the nanowires was metallic Cu. The red, orange, and yellow regions in the chemical state mapping indicate the presence of Cu metal, Cu_2O, and CuO, respectively (Fig. 11 (b), (c)). Although the copper on the surface parts of nanowire was oxidized to Cu_2O and/or CuO, the chemical state inside nanowire was maintained as metal Cu, which corresponds to the foregoing TEM analyses. Based on these observations, we speculate that these Cu nanowires have electrical conducting properties.

Chemical state of Cu	Peak intensity ratio ($I_{L\alpha}/I_{L\beta}$)
Cu (Cu^0)	7.9
Cu2O (Cu^{1+})	5.8
CuO (Cu^{2+})	4.3

Table 1. The peak intensity ratio of $I_{L\alpha}/I_{L\beta}$ of various copper oxide compounds.

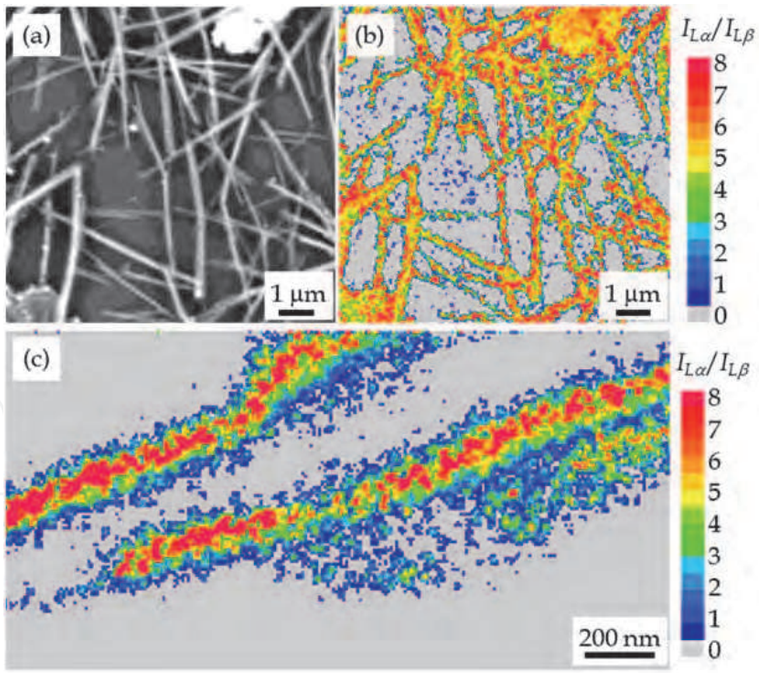

Fig. 11. Chemical state mapping on the cross-sectional surface of Cu nanowires. Backscattering electron image of the same area was also shown (a). The mappings are shown in two different scales: low-magnification (b) and high-magnification image (c) for the same area. Color bar indicates the peak intensity ratio of $I_{L\alpha}/I_{L\beta}$ X-ray fluorescence spectra of Cu.

We have also confirmed that the nanospheres after long time laser irradiation in ethanol are composed of metallic Cu. Fig. 12 shows TEM observations of Cu nanospheres after femtosecond laser irradiation for 20 minutes in ethanol. A1 and A2 arrows in Fig. 12 (a) show the analysis points of the electron energy-loss spectroscopy (EELS). The EELS spectra near the C-*K* and Cu-*L* edges indicate that the Cu nanospheres are covered by a carbon layer (Fig. 12 (b), (c)). Results of the existence of the many metallic Cu nanospheres in the case of long time laser irradiation (Fig. 4 (e), (f)) indicate that these carbon layers, which could be produced by the photo-dissociation of the surrounding solvent molecules, act as a passivation layer preventing not only the aggregation and growth but also their oxidation. Through our experiments, it was found that the dispersed solvent was sensitive to the evolution of morphology of micro-flakes under laser irradiation. Methanol and ethanol were found to be suitable for producing the one-dimensional nanoparticles, such as nanowires and nanorods, while only spherical-like nanoparticles with diameters of about 40 nm were fabricated in the acetone and propanol solution. Moreover, there was no distinct change of the Cu nanospheres after storage in the methanol and ethanol solution for one month.

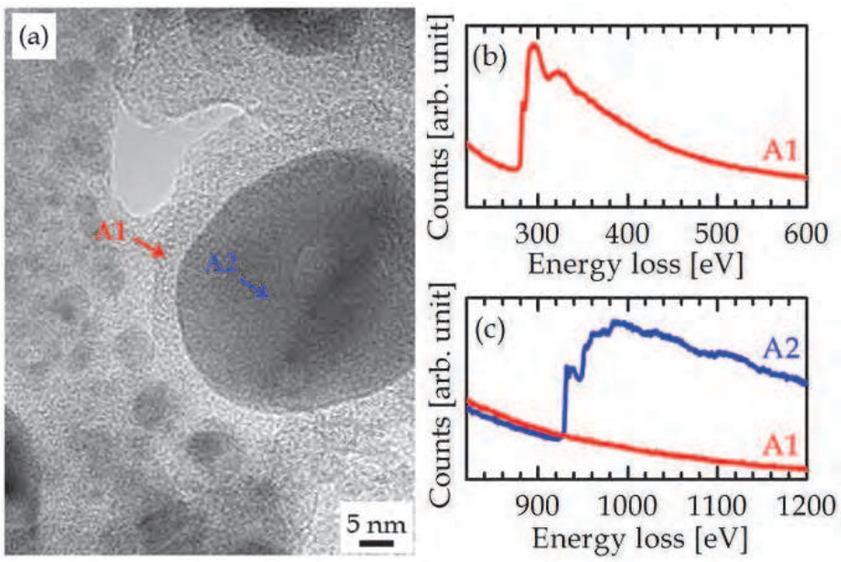

Fig. 12. (a) TEM observations of Cu nanospheres after femtosecond laser irradiation for 20 minutes in an ethanol. Arrows A1 and A2 in image show the analysis points of the electron energy-loss spectroscopy. The electron energy-loss spectra near C-*K* (b) and Cu-*L* edge (c) corresponding to the A1 and A2 arrows are also shown.

2.3 Morphology control factors of Cu nanoparticle

Fig. 13 shows the absorption spectra of the Cu micro-flakes dispersed in ethanol just after linearly or circularly polarized femtosecond laser irradiation for 5 minutes. The absorption spectra after a subsequent aging treatment at room temperature for 5 days are also shown. In each polarization case, absorptions peaking at 600 nm due to the surface plasmon resonance of Cu nanospheres are observed just after laser irradiation. An apparent difference in absorption spectra was observed after a subsequent aging treatment for 5 days. In the case of the circularly polarization, the maximum absorption was shifted to the short

wavelength region (Fig. 13 (b)). This is attributed to the fact that the partial oxidation of Cu nanospheres causes the blue shift (Tilaki et al., 2007). On the other hand, a particular absorption peaking at 380 nm was observed after linearly polarized laser irradiation and subsequent aging treatment (Fig. 13 (a)).

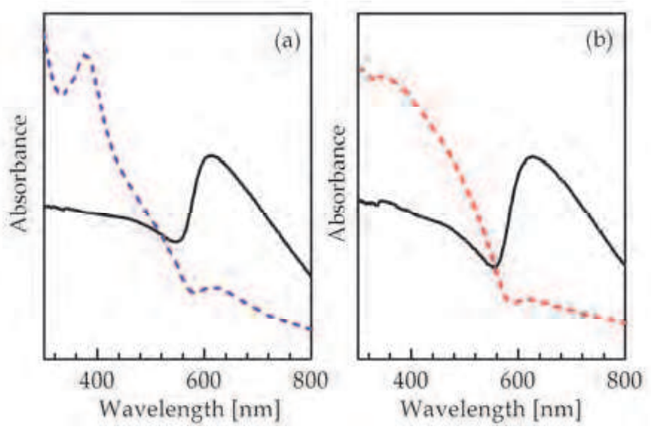

Fig. 13. Absorption spectra of the Cu micro-flakes dispersed in ethanol just after linearly (a) or circularly (b) polarized femtosecond laser irradiation for 5 minutes (solid line). The absorption spectra after subsequent aging treatment at room temperature for 5 days are also shown (broken line).

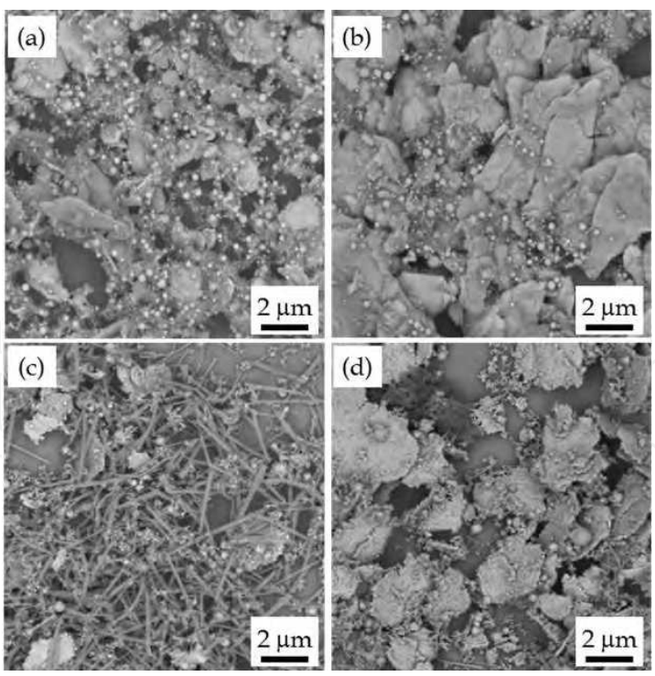

Fig. 14. SEIs of the Cu nanoparticles corresponding to the absorption spectra in Fig. 13. (a) just after linearly polarized laser irradiation and (c) subsequent aging treatment at room temperature for 5 days, (b) just after circularly polarized laser irradiation and (d) subsequent aging treatment at room temperature for 5 days, respectively.

Fig. 14 shows the SEIs of Cu nanoparticles corresponding to the absorption spectra in Fig. 13. In each polarization case, the nanospheres and unreacted starting Cu micro-flakes are observed just after laser irradiation (Fig. 14 (a), (b)), while nanowires can be observed only after linearly polarized laser irradiation and a subsequent aging treatment (Fig. 14 (c)). On the other hand, in the case of circularly polarized laser irradiation, there is no observation of nanowires just after laser irradiation and the subsequent aging treatment (Fig. 14 (b), (d)). These results indicate that the absorption peaking at 380 nm may be due to the surface plasmon resonance of partially-oxidized Cu nanowires. Indeed, it is well-known that the surface plasmon resonance frequencies depend not only on the size but also the shape of particles (Yim et al., 2007).

Why are the nanowires not formed in the case of the circular polarization? In order to understand detailed mechanism of the Cu nanowire formation, we compared experimental results to the finite difference time domain (FDTD) calculation of surface plasmon polariton (SPP) wave propagating along the surface of the Cu nanosphere in an ethanol. Furthermore, the TEM observations of the fragmented Cu nanoparticles just after the linear polarized and the circular polarized femtosecond laser pulse irradiation for 5 minutes in ethanol were performed (Fig. 15 (a), (b)). The ethanol suspended Cu nanoparticle was immediately evaporated at room temperature in order to quench particle growth; therefore, these images may indicate the pre-grown Cu nanoparticle. The differences in the shape of these pre-grown Cu nanoparticles evidently depend on the laser polarization (Fig. 15 (a), (b)). Fig. 15 (c) and (d) show FDTD simulation results of electric field amplitude of the SPP wave excited by the linear polarized and the circular polarized light. In this simulation, we used an input

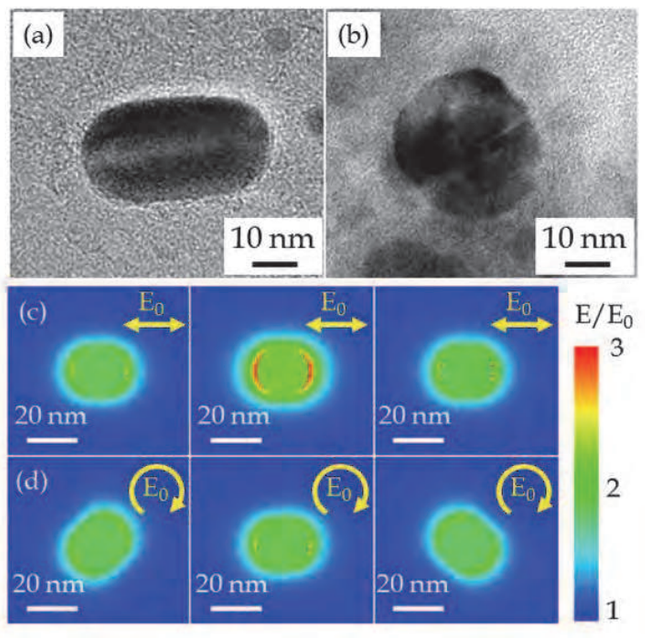

Fig. 15. TEM observations indicating of Cu nanoparticles just after the linear polarized (a) and the circular polarized (b) femtosecond laser pulse irradiation for 5 minutes in ethanol. FDTD simulation results of electric field amplitude of the SPP wave excited by the linear polarized (c) and the circular polarized (d) light are also shown. Each row in (c) and (d) from left to right corresponds to the time domain sequence.

electric field amplitude of $E_0 = 2.4 \times 10^{11}$ V/m corresponding to the laser energy fluence of 2.4×10^3 J/cm^2, a wavelength of 800 nm, and a diameter of Cu nanosphere of 20 nm. In the case of linearly polarized radiation, the localized enhancement of the electric field along the light polarization can be expected (Fig. 15 (c)), while the region of the electric field enhancement rotates according to the circular polarization (Fig. 15 (d)). Such localized enhancement around the Cu nanosphere in the linear polarization induces an anisotropic distribution of the nonlinear photoionization of the Cu nanosphere, resulting in the anisotropic shape modifications.

Stalmashonak and co-workers have also reported that the laser induced shape modification of spherical Ag nanoparticles embedded in soda-lime glass was evoked by the surface plasmon assisted photoelectron emission of the electrons from the metal surface during femtosecond laser irradiation (Stalmashonak et al., 2009). They have also found that such transformation of the metal nanoparticles in glass, which takes place within a timescale of 1 ns, depends on the applied laser pulse intensity, and suggested that the directional memory is defined by the directed emission of hot electrons interacting with the laser field (Unal et al., 2009). Comparing experimental results with simulation results, the shape of the pre-grown Cu nanoparticle produced by the single laser pulse was defined by the laser polarization. Especially, Cu nanoparticles, which act as a nucleation site for Cu nanowire growth, were elongated in the direction parallel to the linear laser polarization. On the other hand, spherical Cu nanoparticles formed by irradiation with the circularly polarized pulses cannot grow into Cu nanowires. We have also confirmed that the one-dimensional growth of Cu nanoparticles occurs during the subsequent aging process.

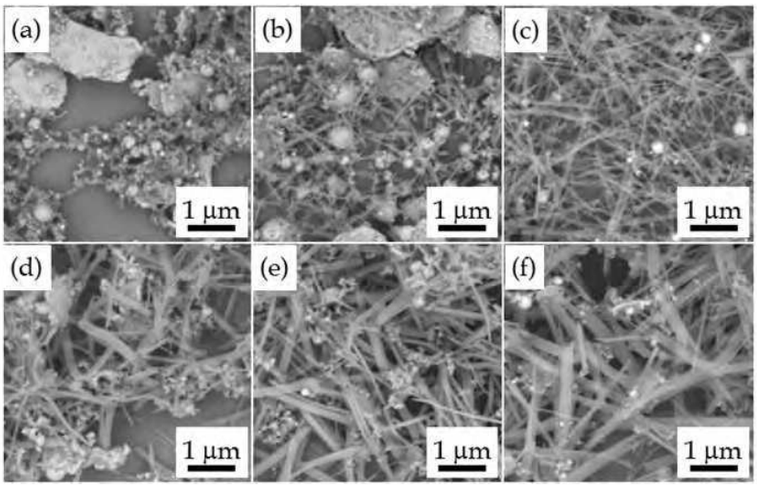

Fig. 16. SEIs of the Cu nanoparticles after linearly polarized femtosecond laser irradiation for 5 minutes and subsequent aging treatment at 40 °C (a) ~ (c) and 60 °C (d) ~ (f). Aging time was 12 hours (a), (d), 24 hours (b), (e), and 120 hours(c), (f), respectively.

Fig. 16 shows SEIs of the Cu nanoparticles after 5 minutes of the linearly polarized laser irradiation and subsequent aging treatment at 40 and 60 °C for several hours. These SEM observations reveal the diameter growth rate of Cu nanowires increases with the aging temperature (Fig. 16). In the initial stage during aging process at 40 °C, namely one-dimensional growth of Cu nanoparticles, nanoscale web-like aggregates of nanoparticles

were formed (Fig. 16 (a)). This phenomenon is similar to the formation of unusual aggregated structures composed of both crystalline and amorphous silicon nanoparticles by the femtosecond laser ablation in the presence of a background gas (Tull et al., 2006). These nanoscale web-like aggregates are expected to be evolved into Cu nanowires (Fig. 16 (a) ~ (c)). Indeed, the inner part of the Cu nanowires was composed of polycrystalline copper (Fig. 9). Detailed SEM observations indicated the diameter of Cu nanowires was variable as a function of the aging time. After the subsequent aging treatment for 120 hours, the diameters of Cu nanowires were eventually about 68 and 185 nm, and the lengths were about 7.5 and 3.5 μm at the aging temperatures of 40 and 60 °C, respectively. This indicates that the aspect ratio of the Cu nanowires can be controlled by the change of the subsequent aging conditions. As described earlier, the shape of Cu nanoparticles was influenced by the surrounding solution. We have also investigated the effect on the growth of Cu nanoparticles by the surrounding solvent. Although the nanoparticles prepared by 3 minutes of laser irradiation in ethanol were almost wire-like, the fraction of nanospheres increased with the laser irradiation time (Fig. 17 (a), (d)). In contrast, the nanoparticles prepared by the same conditions of laser irradiation in methanol were observed to be cubic nanostructures (Fig. 17 (b)), while nanorods were formed in the case of the long time laser irradiation (20 minutes) (Fig. 17 (e)). Besides, in the case of long time laser irradiation in ethanol and methanol, many nanospheres still exist after a subsequent aging treatment for 5 days (Fig. 17 (d), (e)). However, the one-dimensional growth of the nanoparticles after laser irradiation and a subsequent aging treatment occurred in both the cases of ethanol and methanol but no morphological change was observed in the case of using propanol (Fig. 17 (c), (f)).

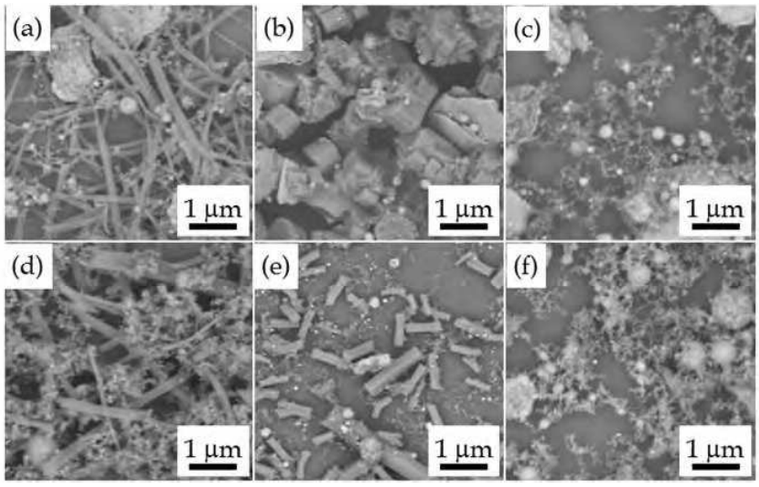

Fig. 17. SEIs of Cu nanoparticles after linear polarized femtosecond laser irradiation for 3 minutes (a) ~ (c) and 20 minutes (d) ~ (f) and a subsequent aging treatment for 5 days in ethanol (a), (d), methanol (b), (e), and propanol (c), (f), respectively.

We speculated that redox state associated with the hydrogen gas generation is also responsible for determining the shape of nanoparticles. To evaluate this assumption, the generated hydrogen gas was detected during laser irradiation. Fig. 18 indicates the hydrogen gas generation rate during femtosecond laser irradiation as a function of the standard enthalpy change of formation, $\Delta_f H°_{liquid}$, of various alcohol solutions. Symbols of •,

▲, ■, and ▼ are experimental data of methanol, ethanol, butanol, and pentanol, respectively. Dotted line indicates a linear fit through the data points. From these results, the hydrogen gas generation rate was evidently proportional to the $\Delta_f H°_{liquid}$ of solvent molecules. In particular, methanol has the most profound inhibitory effect of oxidation. Additionally, an amorphous-like carbon was also produced by the dissociation of solvent molecules. The amount of this photo-dissociation of the solvent is increased with increasing the laser irradiation time and decreasing the length of carbon chain. Such an amorphous carbon could adhere to the surface of the growing Cu particles, and then act as a passivation layer which prevents not only the aggregation and growth but also the oxidation of pre-grown Cu nanoparticles.

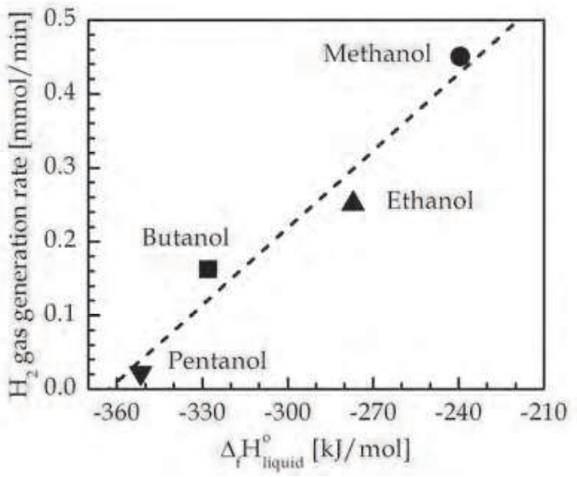

Fig. 18. Hydrogen gas generation rate during femtosecond laser irradiation as a function of the standard enthalpy change of formation, $\Delta_f H°_{liquid}$, of various alcohol solutions. Symbols of •, ▲, ■, and ▼ are experimental data of methanol, ethanol, butanol, and pentanol, respectively. Dotted line indicates a linear fit through the data points.

2.4 Growth mechanism of Cu nanowires

The following explanation of the Cu nanowires' growth is proposed: when an intense femtosecond laser pulse is impinging onto the surface of a metal Cu, multiphoton ionization rapidly occurs without significant ablation. The SPP waves, with a large electric field parallel to the surface, are resonantly excited by light and propagate along the surface. The SPP waves could absorb the light wave via inverse Bremsstrahlung heating (Kupersztych et al., 2004) and couple with the incident light wave only if it propagates in the plane of light polarization. This light-plasma coupling occurs at the flake surface over a narrow region with a depth of the order of the skin depth ($d_p << \lambda$). Previous investigations suggested that either preimposed or self-generated deformations on the solid surface strongly affect laser energy absorption (Feurer et al., 1997). Evidence for small-deformations comes from the wide spreading of the reflected radiation observed in experiments (Zepf et al., 1998). The difference in the light-plasma coupling between linearly and circularly polarized laser pulses should be responsible for different morphology of nanoparticles. Numerical simulations suggested that electron oscillations may grow for a step density profile much faster than the typical time scale of ion motion, leading to an oscillatory "rippling" of the critical surface ($n_e = n_c$) (Macchi et al., 2001).

Such rippling is generated as a result of interference between the light field and the SPP wave launched by initial random surface inhomogeneities. Positive feedback leads to exponential growth of the periodic surface structures oriented perpendicular to the light polarization, which become frozen within the material. The nanowires were also generated by the fragmentation of the initial flakes via interference between the light field and the electric field of the surface plasmon-polariton wave. Indeed, the nanowire formation could not be observed using a circularly polarized beam just after the laser irradiation (Fig. 14, 15). We propose the two successive steps of the Cu nanowire growth mechanism: (1) photofragmentation via interference between the incident light field and the electric field of the SPP wave and (2) nanoparticle growth in a certain direction. Small species of copper such as nanoclusters (and/or atoms) are fragmented from the initial Cu micro-flakes. This process corresponding to the nucleation is affected by the interaction between the electric field of the light wave and the electric field of the excited surface plasmon-polariton wave on the nanoscale. In fact, it is well-known that laser-ablation process of metal target under a liquid environment disperses many types of ablated material, which is called the plume, including small clusters, nanoparticles, free atoms, and ions. Such nanoclusters act as a nucleation site or a source for nanoparticle growth and aggregate into nanoparticles with a larger size compared to the nanoclusters. Self-aggregation of the nanoparticles suspended in the solvent should be prevented by hindering direct contact of the nanoparticles due to the interaction of solvent environment molecules and the surface of nanoparticles. Assuming femtosecond-laser irradiation into a continuous agitation of the suspension, the fragmented Cu nanoparticle with a radius of about 20 nm (Fig. 15) can move at least 86 nm within an interpulse time (τ_{int}) of 1 ms, which was estimated by the Brownian motion of suspended nanoparticles described by the Stokes-Einstein equation:

$$\left\langle \bar{x}^2 \right\rangle = \frac{\kappa_B T \tau_{\text{int}}}{3\pi\eta d} \tag{2}$$

where κ_B, T, η, d are the Boltzmann constant, the temperature, the viscosity of solvent (methanol), and the diameter of the fragmented Cu nanoparticle, respectively. From this estimation, the Cu nanoparticles generated from the initial particles were produced by the single femtosecond laser pulse. Such nucleation site starts growing after the nanoclusters saturate in the solution. Increasing the irradiation time, with more and more nanoclusters being provided at the cost of the micro-flake, the short nanorods on the micro-flake surface keep growing to nanowires. After the micro-flakes are exhausted, no resource can seed the nanoclusters, and then the growth of the nanowires is stopped after consumption of the nanoclusters. At this stage, the laser energy will be absorbed by the nanowires themselves and the nanowires start to fragment into small nanorods and nanospheres due to the drive of the energy of minimization to a more stable morphology (Xiang et al., 2006). After a long irradiation time, nanospheres would become the main product in the methanol solution (Fig. 5 (e), (f)). A similar mechanism of growth was also observed for Se nanowires by using a sonication method (Gates et al., 2002). Although a part of the aggregates are oxidized to Cu_2O, most are kept the metallic state due to reducing environment provided by hydrogen gas generation and covering with the amorphous carbon layer which were photo-dissociated from the surrounding solvent molecules. By the competition between the oxidation to Cu_2O and the aggregation of metallic Cu nanoclusters, Cu nanoparticles grow one-dimensionally into nanowires which have core-shell structure. In fact, it is well known that in the case of Cu_2O crystals, as shown in Fig.19, the O^{2-} ions in the (001) facet are more

apt to hydrolyze, compared with those in the (111) facet, and the stacking along (001) directions therefore becomes energetically favorable (Chen et al., 2003).

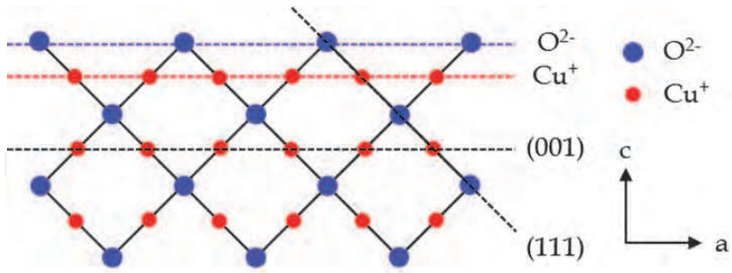

Fig. 19. Projection of the structure of Cu_2O crystal along the [010] direction.

3. Photo-initiated growth of ZnO nanowire

Zinc oxide (ZnO) nanostructures have attracted immense attention as they offer a wide bandgap and a large exciton binding energy of 3.37 eV and 60 meV, respectively, at room temperature (Ohta & Hosono, 2004) and ultraviolet emission (Huang et al., 2001a; Kong et al., 2001; Lin et al., 2007). Various nanostructures such as nanowires (Huang et al., 2001b; Zhang et al., 2005), nanotubes (Zhang et al., 2002a), nanobelts (X. Y. Zhang et al., 2004), nanohelixes, nanosprings and nanorings (Kong & Wang, 2003), nanonails (Kar et al., 2006) and nanodisks (Lin et al., 2007) have been successfully synthesized for various applications such as nanolaser (Huang et al., 2001a), gas sensor (Sberveglieri et al., 2007), biosensor (F. Zhang et al., 2004), field-effect transistor (Arnold et al., 2003), solar cell (Hosono et al., 2005) and field emission (Lee, et al., 2002). A number of physical and chemical synthesis processes have been studied for the growth of ZnO nanostructures. Some of the physical methods include the thermal evaporation and vapor transport approaches (Huang et al., 2001a; Pan et al., 2001), metal organic vapor-phase epitaxial growth (Park et al., 2002), molecular beam epitaxy (MBE) (Heo et al., 2002) and pulsed laser deposition (PLD) (Zhang et al., 2005), which are generally based on catalysed vapor-liquid-solid growth mechanism (Wagner & Ellis, 1964). In addition, the simple and low-cost chemical aqueous solution processing with hydrothermal treatments have also been thoroughly studied (Le et al., 2005; Yang et al., 2006; Zhang et al., 2002a; Zhang et al., 2002b; H. Zhang et al., 2004; X. Y. Zhang et al., 2004). However, all these processes require either high temperature, low pressure, complex procedures, extended growth period or the use of catalysts that could be embedded on the nanostructure tip, which are unfavourable conditions. In this section, a catalyst-free and surfactant-free synthesis process without the above-mentioned adverse conditions, comprising femtosecond laser irradiation to initiate heterogeneous nucleation in aqueous solutions at room temperature and pressure, followed by hydrothermal treatments at low temperatures for crystal growth, is demonstrated. This work exploits pulsed laser to induce nucleation for ZnO nanostructure growth, compared to previously reported laser processing as ablation tools (Zhang et al., 2005).

3.1 ZnO nanorods and nanotubes formation

0.016 M zinc acetate dihydrate ($Zn(CH_3COO)_2{\cdot}2H_2O$) solution was first prepared at room temperature. 0.095 M ammonium hydroxide (NH_4OH) was then added until pH 8 to create

an alkaline environment. By using the above mentioned experimental setup (Fig. 1), the mixture solution was then immediately irradiated with femtosecond pulses with a regeneratively amplified mode-locked Er-doped fiber laser (Cyber Laser Inc.), operating at 780 nm wavelength at 1 kHz repetition rate. The laser beam was focused via a microscope objective (Nikon; LU Plan Fluor, 20× 0.40 N.A.) with typical pulse width and pulse energy of 215 fs and 200 μJ/pulse, respectively, into a rectangular quartz vessel of $1 \times 1 \times 3.5$ cm^3 filled with the pH 8 solution. The vessel was placed on a magnetic stirrer and the solution continuously stirred to maintain homogeneity. Irradiation was performed for 60 minutes and the solution subsequently transferred into furnaces for heat treatments at 60 °C and 80 °C for 120 minutes before being cooled down to room temperature. The grown ZnO nanorods were analyzed by field emission scanning electron microscopy (JEOL, JSM-6705F) to study their morphologies. Samples were prepared by drop-casting the solutions onto silicon substrates and allowed to evaporate at room temperature. X-ray diffraction (XRD) pattern was collected using Rigaku Rint2500HF to study the crystal structure. Room temperature photoluminescence spectrum was obtained via a Horiba Jobin Yvon FluoroMax-P spectrometer with a Xenon lamp excitation source at 300 nm.

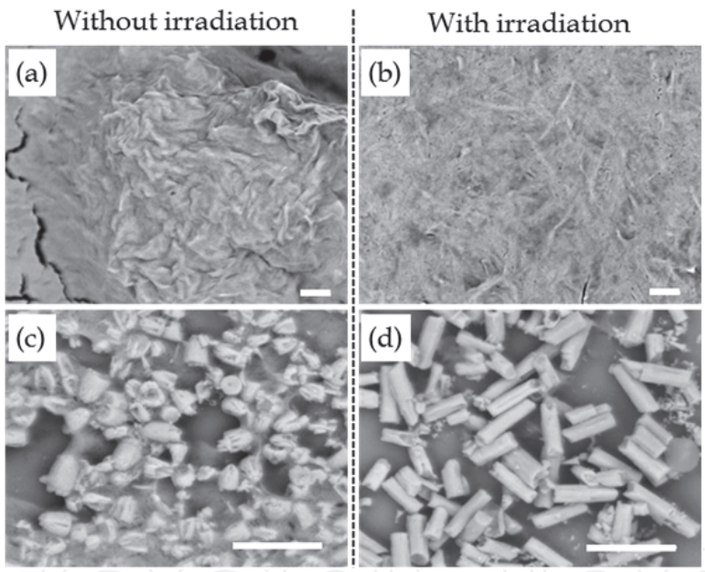

Fig. 20. SEIs of particles in pH 8 solutions without and with laser irradiation at pulse energy 200 μJ/pulse for 60 minutes, after hydrothermal treatments at 60 °C and at 80 °C (c), (d) for 120 minutes. Scale bars are 1 μm.

Fig. 20 (a), (b) and (c), (d) show the SEIs for the pH 8 solutions without and with the laser irradiation process, after hydrothermal treatments at 60 °C and 80 °C, respectively, for 120 minutes. The results show that nanorods were grown only for the solution that underwent irradiation and subsequent treatment at 80 °C. This suggests that the femtosecond pulse irradiation plays a major role in the overall nanorod growth and also, the level of hydrothermal temperature is essential, affecting the solubility of the dissolved zinc species contributing to the ZnO crystal growth. This process shows significantly that no catalyst is required to initiate growth and no surfactant is necessary for preferential nanorod growth direction. Nanorods were grown after hydrothermal treatments for 120 minutes, compared

to previously reported aqueous-based methods requiring more than 10 hours (Yang et al., 2006; Zhang et al., 2002b; H. Zhang et al., 2004). The precipitate observed in Fig. 20 (c) was filtered from the solution, washed, dried at room temperature and analyzed to study the nanostructures in details.

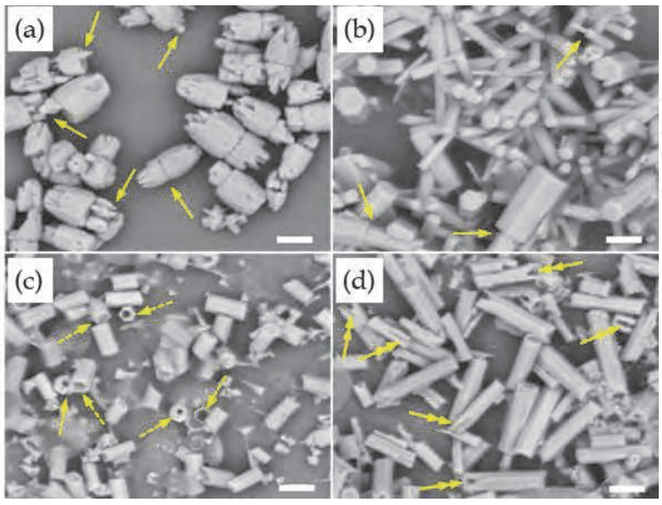

Fig. 21. SEIs for (a) filtered nanoparticles from as-prepared solution after hydrothermal treatment at 80 °C for 120 minutes, without laser irradiation, (b) an aggregation of nanorods and (c), (d) isolated individual nanorods, after irradiation at pulse energy 200 μJ/pulse for 60 minutes and hydrothermal treatment at 80 °C for 120 minutes. Scale bars are 400 nm.

The result, as seen in Fig. 21 (a), shows that without laser irradiation, random homogeneous nucleation could spontaneously occur, leading to the growth of poor quality rod-like nanostructures with rough and porous surfaces. In comparison, Fig. 21 (b) ~ (d) show that large hexagonal nanorods with flat tops and smooth surfaces, with diameters up to 200 nm and lengths up to 1 μm were grown with laser irradiation, which appears to affect the morphology and quality of the nanostructures. We postulate that the femtosecond pulse irradiation initiates heterogeneous nucleation sites, due to induced solution inhomogeneity, acting as seeds for crystal growth into well-structured nanorods with smooth planes during the subsequent hydrothermal treatments where dehydration of the zinc complexation species to ZnO occurs. In addition, the zinc complexation species ions could interact with the laser light polarization and electric field, leading to specific growth directions. The level of hydrothermal temperature is critical and found to be 80 °C for optimal growth. Lower temperature is insufficient to dehydrate the zinc complexation species and no crystal growth is observed (Fig. 20 (b)) while higher temperature could result in the dissolution of the nanorods, leading to poor crystal quality. In Fig. 21 (a), (b), as indicated by arrows, there were instances where smaller secondary nanostructures grew on top of larger primary structures. This is due to additional ZnO nuclei attaching to the top flat surfaces of the primary nanostructures, thereby enabling secondary growth. Eventually, nanorods with lengths up to 1 μm were produced. Other features could also be observed, where the dashed arrows in Fig. 21 (c) indicate nanotubes while the double-headed arrows in Fig. 21 (d) indicate lateral splits along the nanorod side planes. The top plane of the nanorod is the (0001) polar and metastable crystal plane, which could attract hydroxide ions (OH^-). These

OH^- ions attack the plane and erode the central parts of the nanorods, creating nanotubes. Prolonged exposure to OH^- ions could also cause the non-polar and stable crystal side planes to split (Yu et al., 2007).

Fig. 22 (a) shows the XRD pattern for the ZnO nanorods, dispersed on a glass substrate, where the diffraction peaks can be indexed to the ZnO hexagonal structure with a = 3.24 Å and c = 5.19 Å. Fig. 22 (b) shows the idealized (Li et al., 1999) (left) and the actual (right) growth habit observed in this work for the ZnO crystal. For ideal growth, the growth rates of different crystal directions are found to be $V_{<0001>} > V_{<01\bar{1}0>} > V_{<01\bar{1}1>} > V_{<000\bar{1}>}$, with a tip at one end. The appearance of flat tops on the nanorods grown (Fig. 21 (b)) suggests that the growth rate of the (0001) crystal facet is relatively slower than ideal. At pH 8, when NH_4OH is added to $Zn(CH_3COO)_2{\cdot}2H_2O$, the $Zn(NH_3)_4^{2+}$ ammine complexation species is mainly formed as it prevented hydroxide formation and precipitation (Fratesi & Roventi, 1992). As the final growth unit for ZnO is $Zn(OH)_4^{2-}$ (Li et al., 1999), $Zn(NH_3)_4^{2+}$ has to first decompose to $Zn(OH)_4^{2-}$ before dehydration to ZnO at elevated temperature. This intermediate decomposition requires heat, thereby suppressing crystal growth. Hence, $Zn(NH_3)_4^{2+}$ acts as a buffer, slowly releasing the $Zn(OH)_4^{2-}$ growth unit prior to ZnO crystal growth. Furthermore, at pH 8, the nanorods tend to disperse and can be individually identified (Fig. 21) due to the weak basicity of $Zn(NH_3)_4^{2+}$ and the presence of NH_3 which prevent aggregation.

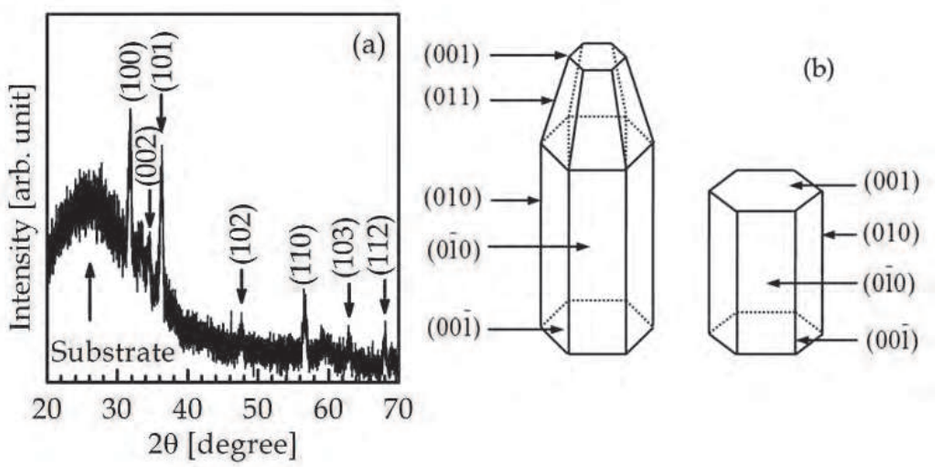

Fig. 22. (a) XRD pattern and (b) growth habits of ZnO nanorods.

Fig. 23 shows the room temperature photoluminescence of ZnO nanorods, with a broad UV emission peaking at ~380 nm that is ascribed to the ZnO band-edge emission due to the recombination of free excitons (Huang et al., 2001b). The broad green emission observed beyond ~530 nm is generally accepted as deep-level or trap-state emission due to radiative recombination of a photogenerated hole with an electron occupying the oxygen vacancy (Vanheusden et al., 1996). The broad spectrum and low intensity observed could be due to poor ZnO crystal quality caused by OH^- attack, the low intensity Xenon lamp source used or the random alignment of the nanorods, resulting in poor luminescence. In addition, coatings of organic solutions could be present on the nanorod surfaces, affecting the results and possibly giving rise to the peaks seen at 450 ~ 470 nm.

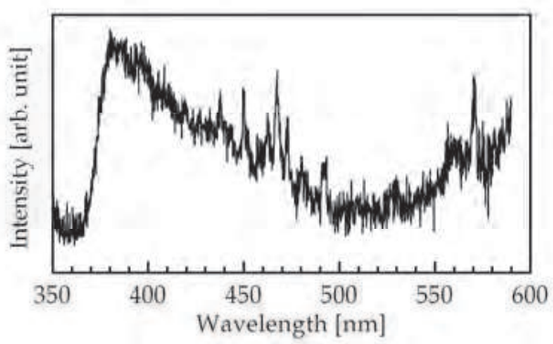

Fig. 23. Photoluminescence spectrum of ZnO nanorods measured at room temperature.

3.2 Role of femtosecond laser irradiation

In order to reveal the role and feasibility of femtosecond laser irradiation in the overall ZnO nanostructure growth process, we performed the following experiments by changing the femtosecond laser irradiation condition (pulse width, pulse energy, and pulse repetition rate). Aqueous mixture solutions of 0.016 M $Zn(CH_3COO)_2{\cdot}2H_2O$ (zinc acetate dihydrate) and 0.20 M NH_4OH (ammonium hydroxide) at a pH value of 11 alkaline environment were initially prepared and then immediately subjected to laser irradiation. The laser radiation in Gaussian mode produced by a regenerative amplified mode-locked Ti:sapphire laser (Coherent Inc., 100 fs pulse duration, 1 kHz or 250 kHz repetition rate) operating at a wavelength of 800 nm was focused by a microscope objective (Nikon; LU Plan Fluor, 20× 0.40 N.A.) to a spot size of ~ 2.4 μm diameter inside a rectangular quartz vessel of $1 \times 1 \times 3.5$ cm^3 filled with the pH 11 precursor solution. The quartz vessel was placed on a magnetic stirrer and continuously stirred to maintain homogeneity. Tables 2 shows the laser irradiation conditions for the femtosecond pulse irradiation performed at the repetition rates of 1 kHz and 250 kHz. Immediately after the laser irradiation, the solutions were placed in ovens for hydrothermal treatments at 80 °C and 100 °C for 120 minutes for the ZnO crystal growth, before being cooled down to room temperature.

Sample	Pulse repetition rate [kHz]	Pulse energy E_{pulse} [μJ]	Irradiation duration t [min]	Total energy E_T [kJ]
1a	1	50	120	0.36
1b	1	200	30	0.36
1c	1	400	15	0.36
2a	1	100	120	0.72
2b	1	200	60	0.72
2c	1	400	30	0.72
3a	1	200	120	1.44
3b	1	400	60	1.44
4a	1	300	120	2.16
5a	250	0.8	120	1.44
5b	250	1.6	60	1.44
5c	250	2.4	40	1.44

Table 2. Femtosecond laser irradiation conditions at 1 kHz or 250 kHz repetition rate.

Fig. 24 shows the SEIs of the nanostructures grown without and with laser irradiation (pulse energy, E_{pulse} 200 μJ/pulse, irradiation duration 120 minutes, total irradiation energy E_T 1.44 kJ and repetition rate 1 kHz), followed by hydrothermal treatments at 80 °C for 120 minutes. Without the laser irradiation, large flower-like structures comprising aggregated cone-shaped nanostructures can be observed, where their surfaces appear to be rough and porous. When the irradiation process was performed as one part of the synthesis process, ZnO nanowire growth can be observed. This shows that the ultrashort pulse laser irradiation plays a significant role in initiating heterogeneous nucleation sites for nanowire growth, compared to the random homogeneous nucleation process associated with hydrothermal growth without the laser irradiation. In a separate investigation, longer pulses of 860 fs were used for the laser irradiation process, instead of the 100 fs pulses used in this work in order to study the significance of ultrashort pulses for nanowire growth. For the study involving 860 fs (results not shown), short cone-tip nanostructures similar to Fig. 24 (b) were grown instead of thin elongated nanowires that were observed in this work.

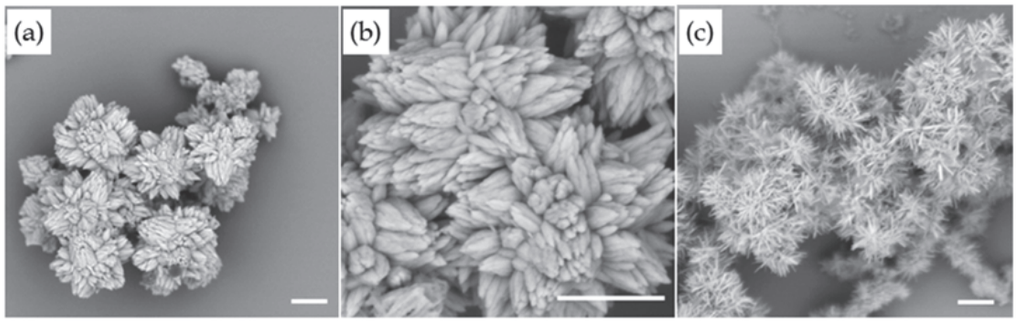

Fig. 24. SEIs of nanoparticles in pH 11 solutions after hydrothermal treatments at 80 °C for 120 minutes, (a), (b) without and (c) with initial laser irradiation at E_{pulse} = 200 μJ/pulse for 120 minutes (E_T = 1.44 kJ) at 1 kHz repetition rate. The laser spot diameter was ~ 2.4 μm. Scale bars are 1 μm.

The generally accepted reaction routes in aqueous ammonia solution at a high alkaline level are defined as below :

$$NH_4OH \leftrightarrow NH_4^+ + OH^- \quad (3)$$

$$Zn^{2+} + 4OH^- \leftrightarrow Zn(OH)_4^{2-} \quad (4)$$

$$Zn(OH)_4^{2-} \leftrightarrow ZnO + H_2O + 2OH^- \quad (5)$$

Upon mixing the starting reagents, the soluble complexation species of $Zn(OH)_4^{2-}$ were formed in a high alkaline environment (pH 11 in this work). Nucleation sites were then produced in the solutions via either random homogeneous nucleation or heterogeneous nucleation by the laser irradiation, which subsequently became aggregated. Acting as the growth units, $Zn(OH)_4^{2-}$ were then dehydrated to ZnO at elevated temperatures to construct the ZnO nanostructures. Fig. 25 summarizes the illustrated scheme for ZnO crystal growth. We postulate that the ultrashort pulse laser irradiation initiates heterogeneous nucleation seeds for subsequent crystal growth during the hydrothermal treatments. During the laser

irradiation process, slight increased in solution turbidity was progressively observed. As similar but increased solution turbidity was observed after the solution was subjected to hydrothermal treatment which caused the dehydration of the zinc complexation species to ZnO, it can be inferred that the ultrashort pulses acted in a similar way to form ZnO heterogeneous nucleation seeds during the laser irradiation process. As seen in Fig. 24, these ZnO heterogeneous seeds lead to nanowire growth compared to homogeneous nucleation seeds. Hence, the laser-induced nucleation affects the morphology of the ZnO nanostructure grown. In addition, it might be possible that the complexation species interact with the light polarization and the electric field of the laser, which then direct the nanowire growth in a certain direction.

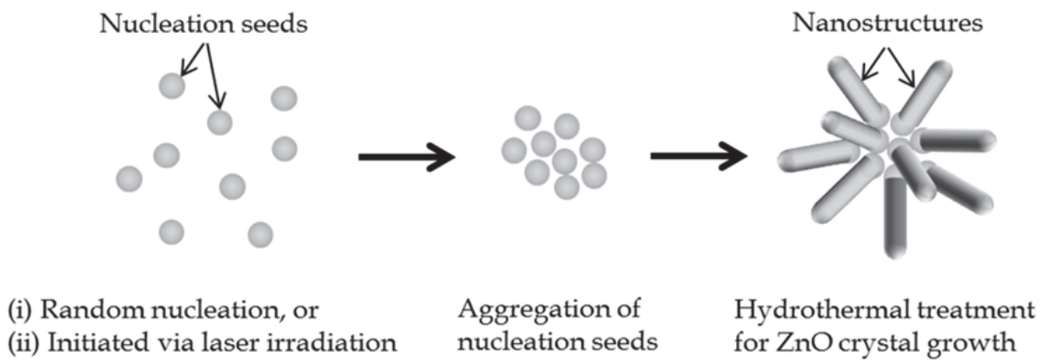

Fig. 25. Schematic representation of the formation of nucleation sites and the growth of ZnO nanostructures in aqueous solutions.

Fig. 26 shows the ZnO nanowires grown from the hydrothermal treatments at 80 °C and 100 °C for 120 minutes, after the laser irradiation at E_T = 0.36 kJ and at 1 kHz repetition rate for different pulse energies (E_{pulse}) and irradiation durations while Fig. 27 shows the results for irradiation at E_T = 0.72 kJ. Fig. 28 shows the ZnO nanowires after the laser irradiation at E_T = 1.44 kJ at E_{pulse} = 200 μJ/pulse for 120 minutes (Fig. 28 (a), (b)) and E_{pulse} = 400 μJ/pulse for 60 minutes (Fig. 28 (c), (d)) and at E_T = 2.16 kJ and E_{pulse} = 300 μJ/pulse for 120 minutes (Fig. 28 (e), (f)), followed by hydrothermal treatments at 80 °C and 100 °C for 120 minutes, respectively. From Fig. 26, we can observe that the pulse energy levels and the hydrothermal treatment temperatures have significant effects on the growth of ZnO nanowires. By comparing the results after hydrothermal treatments at 80 °C and 100 °C for 120 minutes, there are higher density of nanowires grown at 100 °C, which are also more well-defined and longer. This is due to the higher solubility and mobility of the zinc growth units at a higher temperature, which encourages crystal growth. Analysing the results based on pulse energy, well-defined individual nanowires can be observed in the samples after the laser irradiation at E_{pulse} = 200 μJ and 400 μJ, where they are arranged in a flower-like configuration aggregated at one end. This shows that a minimum of E_{pulse} = 200 μJ pulse energy is required to initiate heterogeneous nucleation for nanowire growth. Typical nanowire structure can be observed after the laser irradiation at E_{pulse} = 50 μJ but individual nanowires were not clearly separated from each other. As indicated by arrows in Fig. 26 and the subsequent figures, there are instances where individual nanowires

fused together, possibly via oriented attachment (Pacholski et al., 2002), into larger nanowires. In Fig. 27, the results show that irradiation with E_{pulse} = 100 μJ produced ZnO nanowires where individual nanowires could not be well-defined, as in the case for E_{pulse} = 50 μJ in Fig. 26 (b). Increasing E_{pulse}, while maintaining E_T = 0.72 kJ by reducing the irradiation duration, produced well-defined and individually separated nanowires. This again shows the critical role of E_{pulse} in initiating conducive nucleation sites for crystal growth. In Fig. 28, individual nanowires can be clearly observed for all samples as the threshold E_{pulse} = 200 μJ required to initiate heterogeneous nucleation for favourable growth into ZnO nanowires was exceeded.

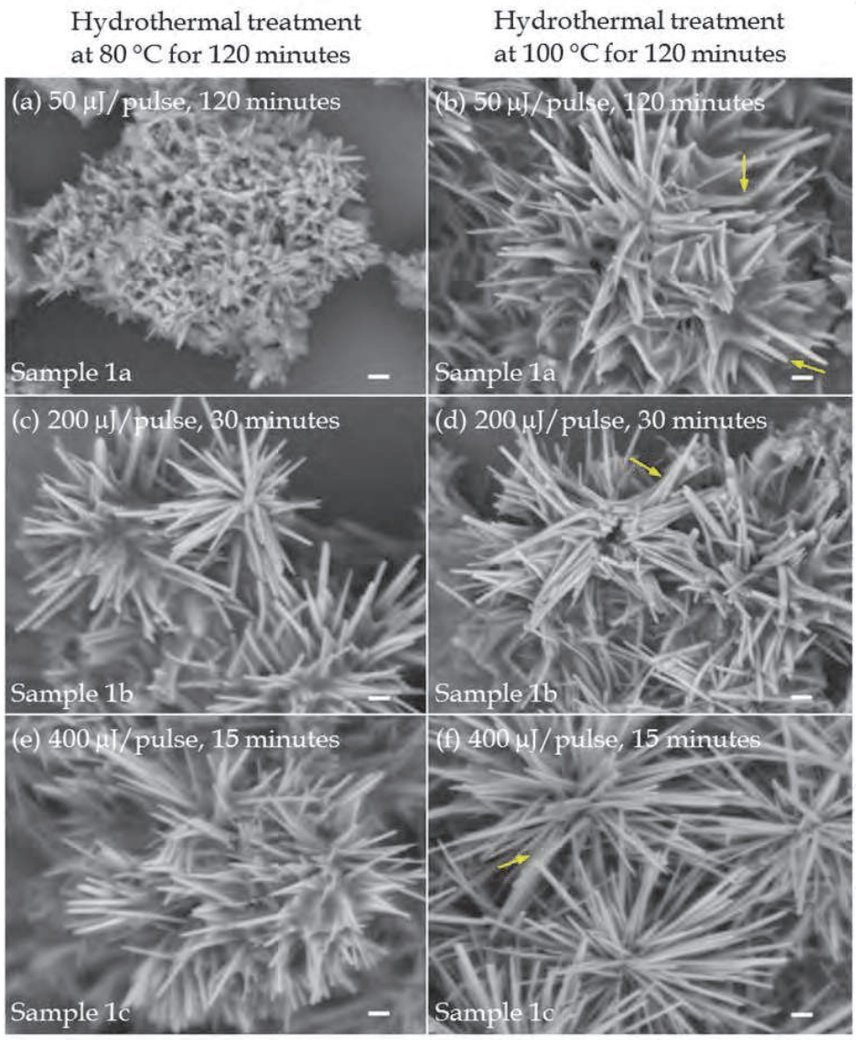

Fig. 26. SEIs for ZnO nanowires grown from ultrashort pulse irradiation at 1 kHz at (a), (b) E_{pulse} = 50 μJ/pulse for 120 minutes, (c), (d) 200 μJ/pulse for 30 minutes, and (e), (f) 400 μJ/pulse for 15 minutes (similar E_T = 0.36 kJ), followed by hydrothermal treatments at 80 °C for 120 minutes (left images) and at 100 °C for 120 minutes (right images). Scale bars are 200 nm.

From the results in Fig. 26 ~ 28, it can be inferred that the pulse energy level, E_{pulse}, is essential in initiating heterogeneous nucleation while the irradiation duration (and indirectly the total irradiation energy, E_T) determines the density of nanowire growth due to the abundant nucleation sites initiated. In addition, these two factors together with the hydrothermal treatment temperature affect the morphology of the nanowires as the rates of dehydration and consumption of the zinc growth units for numerous crystal growth processes would be affected. Generally, based on the amount of zinc growth units available in the quartz vessel and depending on the laser processing parameters and hydrothermal treatments conditions, ZnO nanowires with diameter 10 ~ 40 nm and length up to 1.5 μm can be grown.

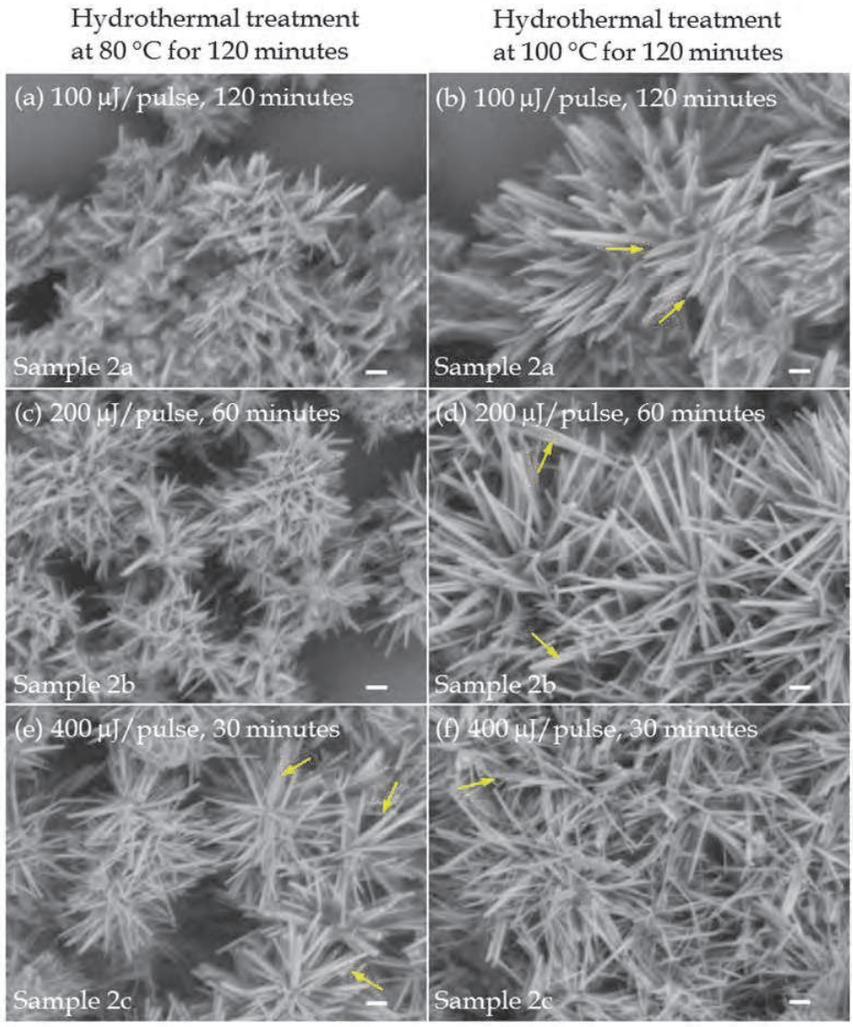

Fig. 27. SEIs for ZnO nanowires grown from ultrashort pulse irradiation at 1 kHz at (a), (b) E_{pulse} = 100 μJ/pulse for 120 minutes, (c), (d) 200 μJ/pulse for 60 minutes and (e), (f) 400 μJ/pulse for 30 minutes (similar E_T = 0.72 kJ), followed by hydrothermal treatments at 80 °C for 120 minutes (left images) and at 100 °C for 120 minutes (right images). Scale bars are 200 nm.

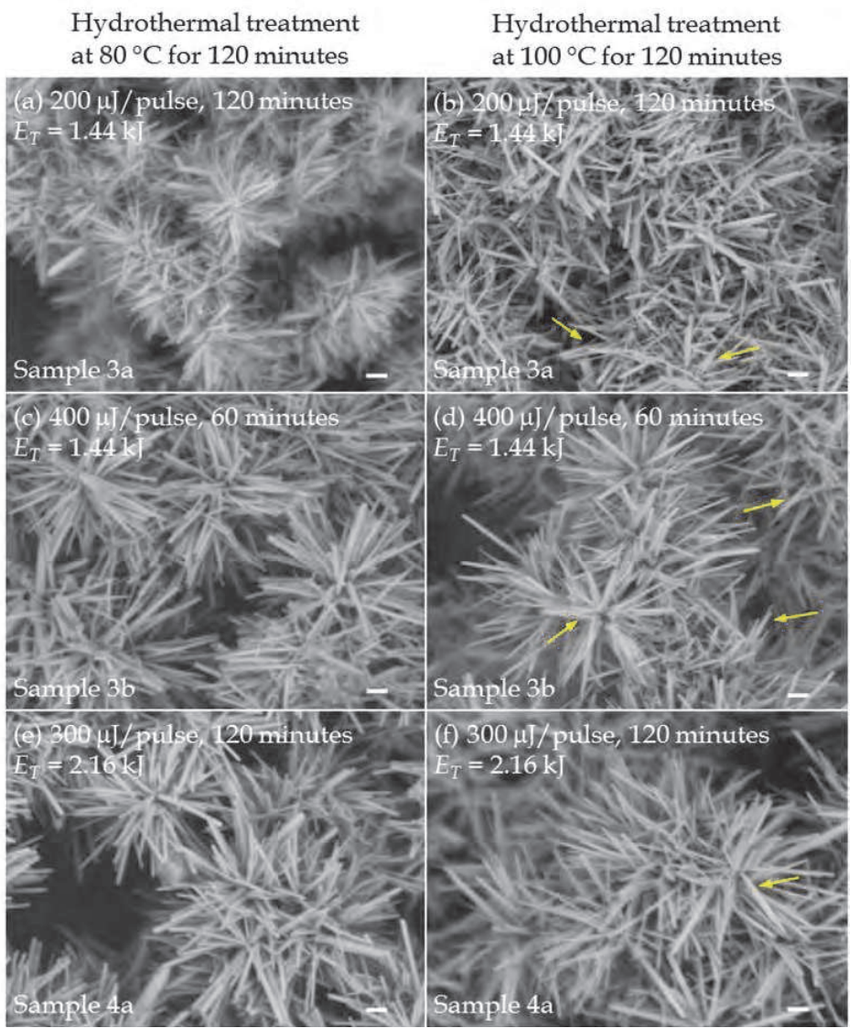

Fig. 28. SEIs for ZnO nanowires grown from ultrashort pulse irradiation at 1 kHz at (a), (b) E_{pulse} = 200 μJ/pulse for 120 minutes and (c), (d) 400 μJ/pulse for 60 minutes (similar E_T = 1.44 kJ) and (e), (f) E_{pulse} = 300 μJ/pulse for 120 minutes (E_T = 2.16 kJ), followed by hydrothermal treatments at 80 °C for 120 minutes (left images) and at 100 °C for 120 minutes (right images). Scale bars are 200 nm.

Fig. 29 summarises the results on ZnO nanowire synthesis after the laser irradiation at E_T = 1.44 kJ at 250 kHz repetition rate for different E_{pulse} values and irradiation durations, followed by hydrothermal treatments at 80 °C and 100 °C for 120 minutes. For irradiation at E_{pulse} = 0.8 μJ/pulse for 120 minutes, the ZnO nanostructures appear to have grown from random homogeneous nucleation similar to that of Fig. 24 (a), (b), suggesting that the low pulse energy had not been effective in initiating heterogeneous nucleation. For the laser irradiation at E_{pulse} = 1.6 μJ/pulse for 60 minutes, the general shape of nanowires can be observed while the results for E_{pulse} = 2.4 μJ/pulse for 40 minutes clearly show aggregations of ZnO nanowires. The difference in morphology and density of nanowires is most likely caused by the abundant nucleation seeds initiated by the higher pulse energy. At E_{pulse} = 1.6 μJ/pulse, the soluble $Zn(OH)_4^{2-}$ species were consumed by less nucleation seeds, leading

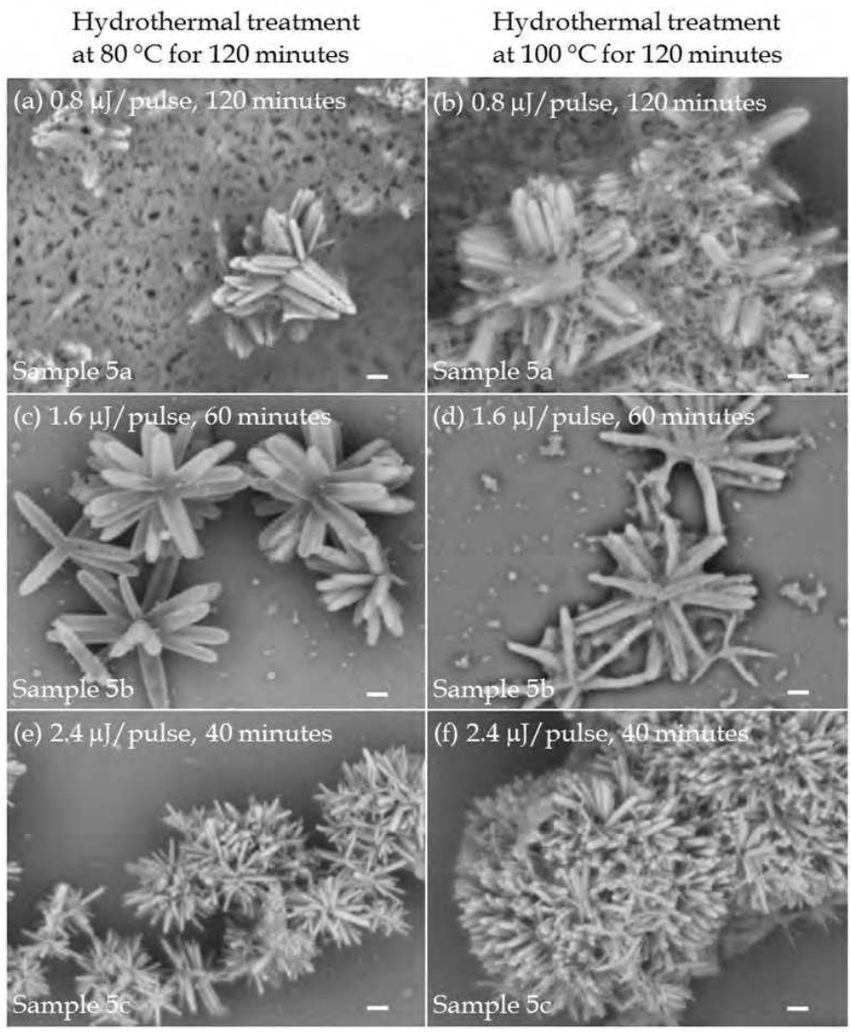

Fig. 29. SEIs for ZnO nanowires grown from ultrashort pulse irradiation at 250 kHz at (a), (b) E_{pulse} = 0.8 μJ/pulse for 120 minutes, (c), (d) 1.6 μJ/pulse for 60 minutes and (e), (f) 2.4 μJ/pulse for 40 minutes (similar E_T = 1.44 kJ), followed by hydrothermal treatments at 80 °C for 120 minutes (left images) and at 100 °C for 120 minutes (right images). Scale bars are 200 nm.

to large nanowire dimensions. However, at E_{pulse} = 2.4 μJ/pulse, the $Zn(OH)_4^{2-}$ growth units were consumed and distributed over a larger amount of nucleation sites for growth and thus reducing the dimensions of the nanowires grown. In addition, at E_{pulse} = 1.6 μJ/pulse, the pulse energy might be too low to initiate stable heterogeneous nucleation so that two or more nucleation seeds might have merged to produce a larger seed and consequently the larger dimensions for the nanowires. This is highly likely due to the high frequency of pulses which initiate high amount of nucleation seeds in close proximity, thus enabling neighbouring seeds to merge to improve stability. This dependence of nanowire diameter on the size of the nucleation seeds is similar to the correlation between nanowire diameter and gold nanodot size, which acted as catalysts, observed by Fan et. al. (Fan et al., 2006). The high number of nucleation seeds near each other also enables them to produce large

aggregations of nanowires, as seen in Fig. 29 (f), compared to those grown from 1 kHz repetition rate laser irradiation. Finally, homogeneous nucleation might have also played a part in the growth process for Fig. 29 (c), (d), which has been shown to produce larger nanostructures compared to that grown purely from heterogeneous nucleation. These large differences in the results in Fig. 29 suggest that there is a certain threshold level for E_{pulse} to initiate nucleation sites in the solution. The results also agree with the results obtained via laser irradiation at the repetition rate of 1 kHz, which showed the significant role of E_{pulse}. In addition, comparing the results of Fig. 26 ~ 29 show that well-defined nanowires could be grown beyond E_{pulse} = 2.4 μJ/pulse at 250 kHz repetition rate. However, at 1 kHz repetition rate, E_{pulse} beyond 200 μJ/pulse was required for well-defined ZnO nanowire growth. This difference in E_{pulse} level could be attributed to the thermal effect induced by irradiation at 250 kHz repetition rate.

Fig. 30 shows the illustrated temperature profiles expected in the sample solutions irradiated by 1 kHz and 250 kHz ultrashort pulses. The thermal diffusion time was estimated to be approximately 3 μs using the thermal diffusion equation (Chartier & Bialkowski 1997), based on a laser spot radius of 1.22 μm estimated by the Airy disc approximation (Vogel et al., 2005) and the heat diffusivity of water = 1.38×10^{-7} m^2 s^{-1} (Vogel et al., 2005). As seen in Fig. 30, the diffusion time is of the same order as the pulse interval for the 250 kHz pulses and hence thermal effect would be expected to build up within the localised laser spot volume and possibly contribute to the heterogeneous nucleation process. In contrast for the train of 1 kHz pulses, thermal effect was negligible as the heat induced by a single pulse would have completely dissipated by the time the next pulse arrived 1 ms later.

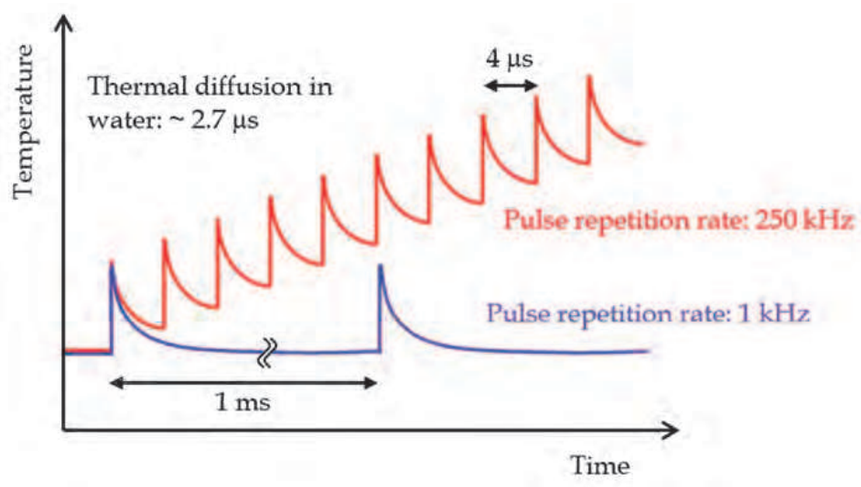

Fig. 30. Temperature profiles induced in the irradiated samples by femtosecond laser pulses at repetition rates of 1 kHz and 250 kHz.

3.3 Formation mechanisms of ZnO nanorods

In order to reveal the formation mechanisms of ZnO nanorods with the additional femtosecond laser irradiation process, we performed the following experiments. Aqueous mixture solutions of 0.02 M $ZnCl_2$ and 0.032 ~ 0.200 M NH_4OH at pH value ranging from 8.5 to 10.5 alkaline environments were initially prepared. We used femtosecond laser pulses to focus in a liquid cell and efficiently transfer energy into the precursor solution. The initial

solution exhibits a slightly white turbidity decreasing with a pH increase because the formation of zinc ammonia complex, which was subjected to femtosecond pulse irradiation at room temperature. The laser radiation in Gaussian mode produced by a regenerative amplified mode-locked Er-doped fiber laser (Cyber laser Inc., 230 fs pulse duration, 1kHz repetition rate, pulse energy 0.5 mJ/pulse) operating at a wavelength of 780 nm was focused by an objective (Nikon; LU Plan Fluor, 20× 0.40 N.A.) into a rectangular quartz vessel of 1 × 1 × 3.5 cm^3 filled with the precursor solution, which was placed on a magnetic stirrer and continuously stirred to maintain homogeneity. Irradiation was performed for 60 min and the solution subsequently transferred into furnace for heat treatments at 80 °C or 100 °C for 120 minutes before being cooled down to room temperature. Samples were prepared by drop-casting the solutions onto silicon substrates and allowed to evaporate at room temperature. The grown ZnO particles were analyzed by field emission scanning electron microscopy (JEOL JSM-6705F) to study their morphologies. X-ray diffraction (XRD) pattern was collected using Rigaku Rint2500HF to study the crystal structure.

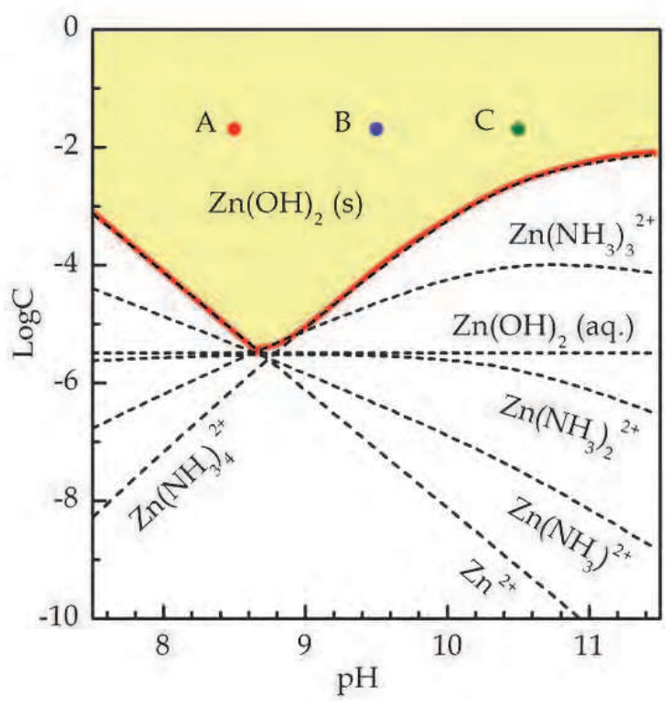

Fig. 31. Phase stability diagram for $Zn(OH)_2$-NH_3 system at 25 °C as a function of pH. The points marked by A, B, and C represent the preparation conditions of precursor solution in this study. The dashed lines indicate the thermodynamic equilibrium between the various Zn(II) soluble species and the solid $Zn(OH)_2$. The red solid line represents the boundary of the solubility of the solid $Zn(OH)_2$.

It is well known that the solid phase stability of $Zn(OH)_2$ in the precursor solution has been determined by the pH value and the concentration of Zn(II) soluble species (Yamabi & Imai, 2002). Fig. 31 shows the phase stability diagrams for the $Zn(OH)_2$−NH_3 systems at 25 °C. The dashed lines indicate the thermodynamic equilibrium between the various Zn(II) soluble species, which are calculated by the following equilibrium equations (6) ~ (8).

$$Zn^{2+} + iNH_3 \leftrightarrow Zn(NH_3)_i^{2+} \quad (6)$$

$$Zn(NH_3)_i^{2+} + 2OH^- \leftrightarrow Zn(OH)_2\,(s) + iNH_3 \quad (7)$$

$$Zn(OH)_2\,(s) \leftrightarrow Zn(OH)_2\,(aq.) \quad (8)$$

Values of standard thermodynamic data and stability constant are taken from the literature (Goux et al., 2005; Hubert et al., 2007; Peulon & Lincot, 1998; Yamabi & Imai, 2002). The red solid line represents the boundary of the solubility of the solid $Zn(OH)_2$. This diagram reveals that the solid $Zn(OH)_2$ is thermodynamically stable at a pH value ranging from 7 to 12 in the precursor solutions ($[Zn^{2+}]$ = 0.02 M). Typical three precursor solutions with different pH values of 8.5, 9.5, and 10.5 were prepared in the present study.

Fig. 32 indicates XRD patterns of precipitates from mixed precursor solutions of $ZnCl_2$ and NH_4OH at pH 8.5, 9.5, and 10.5 without (a) and with (b) the femtosecond laser irradiation for 60 minutes and the successive thermal treatment at 80 °C for 120 minutes. The JCPDS standards of $Zn_5(OH)_8Cl_2{\cdot}H_2O$, $Zn(OH)_2$, and ZnO are also shown in Fig. 32.

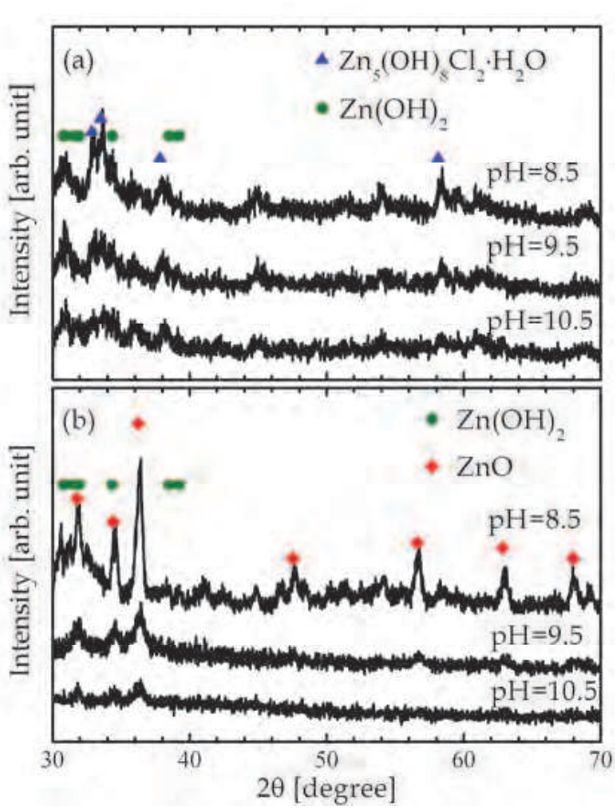

Fig. 32. XRD patterns of precipitates from mixed precursor solutions at pH 8.5, 9.5, and 10.5 without (a) and with (b) the femtosecond laser irradiation for 60 minutes and the successive thermal treatment at 80 °C for 120 minutes. The JCPDS standards of $Zn_5(OH)_8Cl_2{\cdot}H_2O$ (▲), $Zn(OH)_2$ (●), and ZnO (■) are also shown.

The corresponding SEIs are shown in Fig. 33. No apparent diffraction peaks of ZnO were observed in the case of the thermal precipitates from precursor solutions at every pH

condition without the laser irradiation (Fig. 32 (a)). These patterns were assigned to $Zn(OH)_2$ and $Zn_5(OH)_8Cl_2{\cdot}H_2O$, suggesting that the precursor solutions could not become supersaturated at 80 °C with respect to the homogeneous ZnO nucleation. On the other hand, the apparent diffraction peaks attributed to ZnO were observed in the samples which the laser irradiation process was applied before thermal treatment at the same temperature (Fig. 32 (b)). This indicates that the photo-initiated heterogeneous nucleation could be induced by the femtosecond laser irradiation in the precursor solutions at room temperature. The SEIs in Fig. 33 evidently indicate that in contrast to the formation of the scale-like or amorphous precipitate after the thermal treatment at 80 °C for 120 minutes, the ZnO hexagonal nanorods with a diameter of 40 ~ 80nm, which slightly decreases with a pH increase, were obtained by applying the laser irradiation (Fig. 33 (d) ~ (f)). Based on these results, we speculated that the nucleations of ZnO nanorods were initiated by the local supersaturation via femtosecond laser pulse irradiation even at the room temperature.

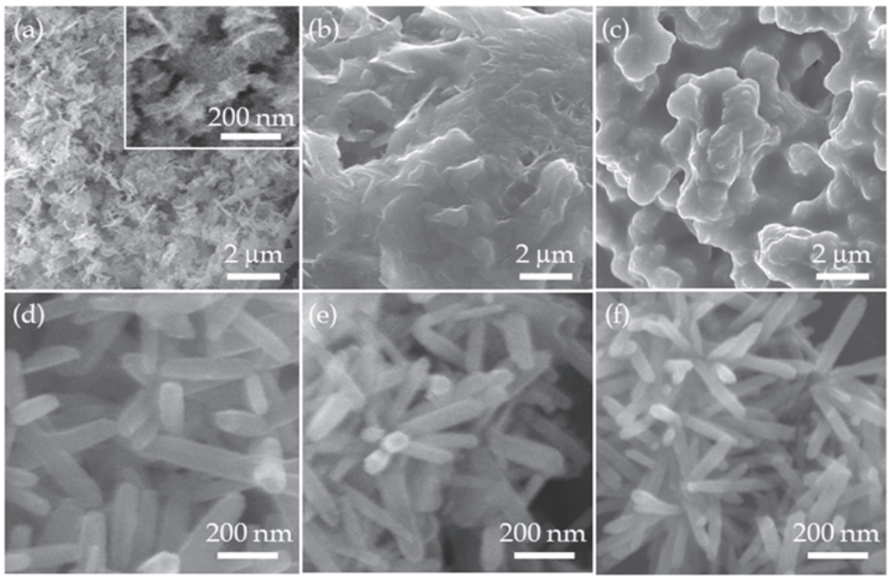

Fig. 33. SEIs of precipitates synthesized from mixed precursor solutions at pH 8.5 (a), (d), 9.5 (b), (e), and 10.5 (c), (f) by the thermal treatment at 80 °C for 120 minutes (upper row) and the additional femtosecond laser irradiation before the thermal treatment (lower row). Inset of (a) shows a high magnification image of scale-like particles.

In order to reveal the nucleation and growth mechanisms of ZnO nanorods with the additional femtosecond laser irradiation process, the heating temperature during the successive thermal treatment was changed to 100 °C. ZnO nanoparticles were precipitated with or without laser irradiation (Fig. 34). The shape of ZnO nanoparticles was changed from nanorods to flower-like with increasing the pH in the thermal treatment (Fig. 34 (a), (c)). In addition, the smaller ZnO nanoparticles resulting from secondary nucleation were observed at the pH of 9.5 (Fig. 34 (b)). It is well known that the flower-like ZnO nanostructures are formed via twinned ZnO nuclei along the $(1\bar{1}22)$ planes in the system with higher supersaturation of $Zn(OH)_4^{2-}$ (Zhang & Mu, 2007). On the other hand, much smaller ZnO nanorods with a diameter of 20 ~ 70 nm were formed by the additional laser

irradiation compared to that of the thermal process regardless of pH, about 4 times thinner nanorods were especially formed at the pH of 8.5 (Fig. 34 (a), (d)). The size of ZnO nanorods obtained by the laser irradiation increased with an increase in pH (Fig. 34 (d) ~ (f)). Comparison of the effect of temperature on the size of ZnO nanorods between 80 °C and 100 °C with the laser irradiation indicates that the size decreases with increasing temperature at pH of 8.5 and 9.5, although the size increases with increasing temperature at pH of 10.5 (Fig. 33 (d) ~ (f), Fig. 34 (d) ~ (f)).

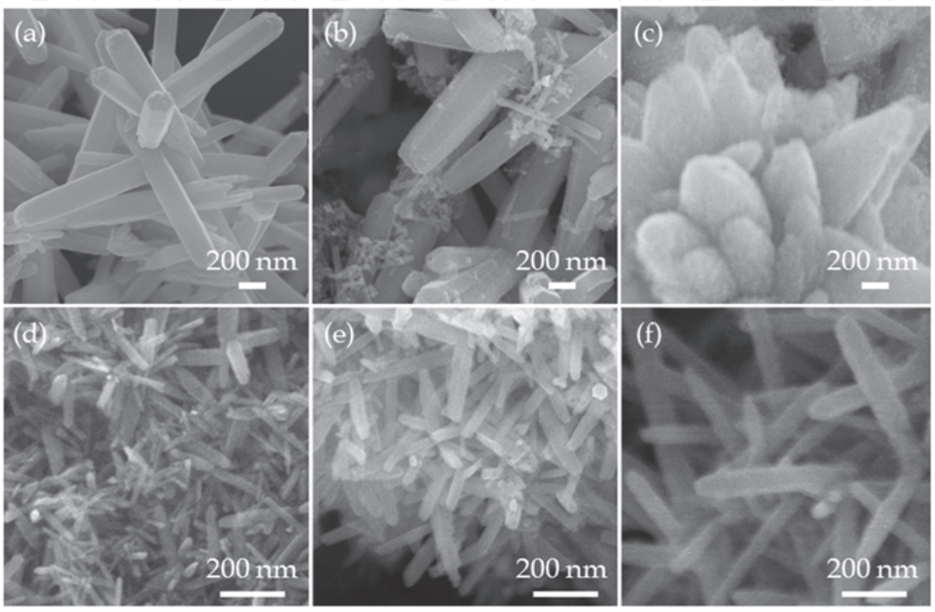

Fig. 34. SEIs of precipitates synthesized from mixed precursor solutions at pH 8.5 (a), (d), 9.5 (b), (e), and 10.5 (c), (f) by the thermal treatment at 100 °C for 120 minutes (upper column) and the additional laser irradiation before the thermal treatment (lower column).

Based on the difference in the shape and size of ZnO nanostructures with and without the femtosecond laser irradiation before the subsequent thermal treatment, we deduce the formation mechanism of ZnO nanorods below. The possible reactions in our experiments can be summarized in the following equations (9) ~ (12).

$$Zn^{2+} + 2OH^- \leftrightarrow Zn(OH)_2\ (s) \tag{9}$$

$$Zn(OH)_2\ (s) \rightarrow ZnO + H_2O \tag{10}$$

$$Zn^{2+} + 4NH_3 \leftrightarrow Zn(NH_3)_i^{2+} \tag{11}$$

$$Zn(NH_3)_4^{2+} + 2OH^- \rightarrow ZnO + 4NH_3 + H_2O \tag{12}$$

In the experimental pH region, we could consider the soluble species of the uncomplexed Zn^{2+} ions and the zinc-ammonia complex ions of $Zn(NH_3)_4^{2+}$ at a much higher concentration of NH_3. In addition, the insoluble compounds of $Zn(OH)_2$ can be formed in this system. The calculated concentration of $Zn(NH_3)_4^{2+}$ and solid $Zn(OH)_2$ in mixed precursor solutions are shown in Table 3.

pH	$Zn(NH_3)_4^{2+}$ [mol/L]	$Zn(OH)_2$ (s) [mol/L]	ZnO nanorods	
			Diameter [nm]	Length [nm]
8.5	8.1 × 10-7	9.1 × 10-3	38 (7) [a]	164 (5) [a]
9.5	7.8 × 10-5	9.1 × 10-3	44 (5) [a]	233 (3) [a]
10.5	2.4 × 10-3	6.6 × 10-3	68 (24) [a]	515 (46) [a]
[a] The numbers in the parenthesis show the standard deviation for 20 samples.				

Table 3. Calculated concentration of soluble and insoluble Zn(II) species and the corresponding the size of obtained ZnO nanorods.

The size of obtained ZnO nanorods produced by the femtosecond laser irradiation at 0.5 mJ for 60 minutes and the successive thermal treatment at 100 °C for 120 minutes are also shown. The amount of such precipitation depends on the pH and the concentration of NH_3 in the solution based on the solubility of $Zn(OH)_2$ and the dissociation constants of $Zn(NH_3)_4^{2+}$. At the pH of 8.5 and 9.5, the reaction of Eq. (9) is dominant and the equilibrium moves to right, namely the nuclei of ZnO are predominantly formed from $Zn(OH)_2$ by the laser irradiation. In contrast, a large amount of the soluble complexes ions of $Zn(NH_3)_4^{2+}$ in addition to the precipitation could be consumed by the formation of ZnO nuclei during laser irradiation, because the reaction of Eq. (11) is dominant at the pH of 10.5. Indeed, the energy absorption by the focusing of femtosecond laser pulses was almost same of 66 % regardless of the pH, although the scattered light intensities at the pH of 8.5 and 9.5 was about 2.5 times higher than that at the pH of 10.5. During the subsequent thermal treatment after the laser irradiation, ZnO nuclei formed by the different reaction path grow into ZnO nanorods along the c-axis direction (Baruah & Dutta, 2009). In lower pH solution (pH 8.5), the smaller ZnO nanorods are formed by the secondary nucleation and growth during the hydrothermal process (Fig. 34 (d)). On the other hand, the larger nanorods could be obtained because ZnO nuclei formed by the laser irradiation grow dominantly during the thermal treatment. It is noted that the standard Gibbs free energy changes of Eq. (10) and (12) are -3.94 and -47.2 kJ/mol, respectively.

To discuss the dynamics of ZnO nuclei formation during the femtosecond laser irradiation, we measured the evolution of spectral extinction of the precursor solutions during the femtosecond laser irradiation (Fig. 35). The transmitted visible light was detected by a photonic multi- channel analyzer (Hamamatsu Photonics, PMA-11). The components of the extinction in Fig. 35 include the sum of light scattering and absorption by ZnO nuclei formed by the laser irradiation. Assuming that the visible absorption of ZnO is negligible, we could estimate the dynamics of the photo-initiated nucleation process based on the Rayleigh scattering theory. In the Rayleigh scattering regime, the scattered light intensity is inversely proportional to the fourth power of wavelength, indicating the shorter wavelength will scatter more than the longer wavelength. While the scattered light intensity in the lower pH solution was substantially constant (Fig. 35 (a)), in the higher pH solution, the scattered light intensity in the shorter wavelength region increases with an increasing in laser irradiation time (Fig. 35 (c)). The results clearly indicate that ZnO nuclei are produced from the liquid phase, i.e. Eq. (11) and (12), in the higher pH solution. On the other hand, the scattering light intensity does not change dramatically because solid $Zn(OH)_2$ already exists in the lower pH solution (Eq. (9) and (10)). Finally, ZnO nuclei produced through different reaction pathways grow into ZnO nanorods during the successive thermal treatment even in the higher pH solution.

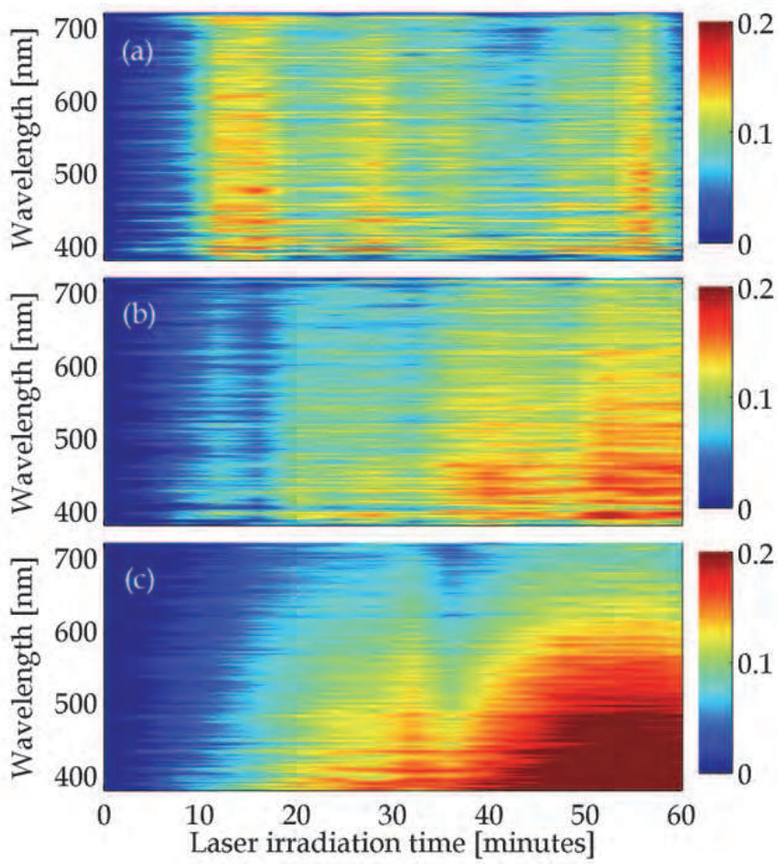

Fig. 35. Evolution of visible extinction spectra of the precursor solution at pH 8.5 (a), 9.5 (b), and 10.5 (c) during femtosecond laser irradiation. The components of the extinction include the sum of light scattering and absorption by ZnO nuclei formed by the laser irradiation.

In order to understand the origin of the observed phenomenon, the following explanation of the heating mechanism is proposed. Since the light intensity in the focus of the beam is of 10^{16} W/cm^2, the plasma is produced by multiphoton ionization in the focal volume. Once a high free electron density is produced by multiphoton ionization, the material has the properties of plasma and will absorb the laser energy via absorption mechanism of inverse Bremstrahlung heating. Assuming that the electron temperature is proportional to the pulse energy, the electron temperature can be roughly estimated by a simple formula: $Q = C_e V T_e$,where Q (= ηE) is the absorbed energy, η is the absorption coefficient, E is the pulse energy, V is the volume interaction, T_e is the electron temperature, and C_e is the electron heat capacity. Within the free electron gas model, The electron heat capacity can be approximately calculated by $C_e(T_e) = \gamma T_e$, where $\gamma = \pi^2 n_e \kappa_B^2 / 2 I_E$ (Lin et al., 2008), where n_e is the electron number density, κ_B is the Boltzmann constant, I_E is the ionization potential. The electron temperature is estimated to be 1.3 keV (~ 1.5×10^7 K) by using the parameters in Table 4, which corresponds to the experimental results (Hatanaka et al., 2004).

Material	Water	-
Density, ρ	1.0×10^{3}	[kg/m^3]
Molar weight, M	1.8×10^{-2}	[kg/mol]
Ionization potential, I_E	6.5	[eV]
Laser wavelength, λ	7.8×10^{-7}	[m]
Pulse width, τ_p	2.3×10^{-13}	[s]
Pulse energy, E	5.0×10^{-4}	[J]
Absorption coefficient, η	0.2	-
Electron density, n_e	1.0×10^{20}	[cm^{-3}]
Numerical aperture, NA	0.45	-

Table 4. Parameter for the calculation of the electron temperature.

Based on this calculation, not only the optical breakdown, bubble formation, but also the dissociation of the precursor solution could occur within the focal volume during the femtosecond laser irradiation. Such very high electron temperature decreases with an increase of the lattice temperature, then it reaches to the same temperature as lattice temperature with a time scale of several picoseconds. Assuming that the initial temperature of focal volume reaches ΔT_0 = 3000 K after the electron-phonon coupling, the thermal diffusivity can be calculated by the following equation. For simplicity, we used the thermal diffusivity coefficient of distill water ($D_{th} = 1.43 \times 10^{-7}$ m^2/s).

$$\Delta T(r,t) = \Delta T_0 \left(\frac{w_0}{\sqrt{w_0^2 + 4D_{th}t}} \right)^3 \exp\left(-\frac{r^2}{w_0^2 + 4D_{th}t} \right) \tag{13}$$

where ΔT_0 is the initial temperature just after the femtosecond single pulse irradiation, w_0 is the laser beam waist, t is the time after the irradiation, and r is the distance from the focus. Fig. 36 indicates the calculated temperature distributions just after the femtosecond single

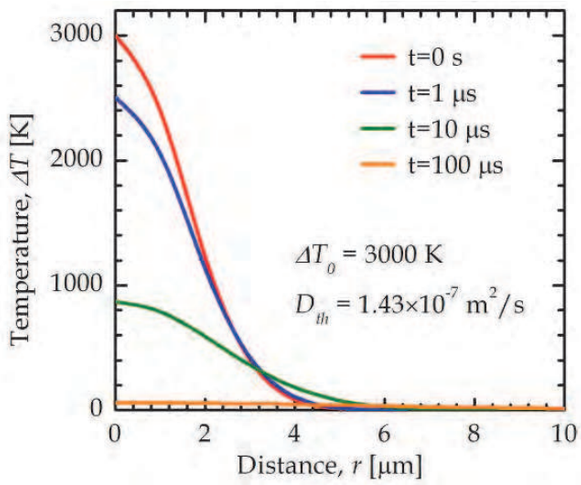

Fig. 36. Calculated temperature distributions just after the femtosecond single pulse irradiation as a function of the distance from focus. In this calculation, the time after the laser irradiation were changed from 0 s to 100 μs.

pulse irradiation as a function of the distance from focus. In this calculation, the time after the laser irradiation were changed from 0 s to 100 μs. Since the repetition rate of 1 kHz, i.e. the interpulse time of 1 ms in the experiments, these calculations apparently indicate that the heat induced by the first pulse can diffuse away from the focal region before the arrival of the successive pulse. Indeed, no apparent temperature change occurred after the femtosecond laser irradiation for 60 minutes. The ZnO nucleation induced by the femtosecond laser irradiation could occur at the instantaneous high-temperature region surrounding the focal volume in precursor solution at room temperature.

4. Conclusion

In conclusion, we have successfully demonstrated the morphological control of Cu nanoparticles by femtosecond laser irradiation in an alcohol solution. Cu nanowires with a core-shell structure are formed depending on the surrounding solvent and laser irradiation time. The aspect ratio of the Cu nanowires can be controlled by a change of the subsequent aging conditions. The evolution of Cu nanowires from micro-flakes in the intense ultrashort light pulses, it was observed that first nanorods appeared on the micro-flake surface, then nanowires at the cost of initial microparticles and finally these were converted to nanospheres. The mechanism of nanowires' growth was suggested to be a nuclear growth mechanism, that is Cu atoms and/or nanoclusters, produced by the femtosecond laser irradiation, then grew into nanorods and finally nanowires. The uniaxial growth mechanisms of Cu nanowires are interpreted in terms of a competition between the oxidation to Cu_2O and the aggregation of metallic Cu nanospheres. Another interesting phenomenon is the polarization-dependence of the formation of Cu nanowires, resulting from interference between the incident light field and the SPP wave. Apart from the fundamental importance of the observed phenomenon, as the first evidence of photofragmentation of Cu nanowires fabricated by the "top-down" approach, could be useful for an optical polarization control medium, an electro-conductive nanomaterial, and a probe for SPM.

Furthermore, ZnO hexagonal nanorods and nanowires were successfully synthesised from heterogenous nucleation initiated by femtosecond laser irradiation in aqueous solutions with subsequent hydrothermal treatments, without catalyst and surfactant. The laser irradiation process improves the morphology and quality of the nanorod crystal compared to porous rod-like structures when no irradiation was performed. Due to the localized high supersaturation of precursor solution, the size of the obtained hexagonal ZnO nanorods with femtosecond laser irradiation and the subsequent thermal treatment is about 4 times thinner than that obtained by the thermal treatment. The nanorods have diameters up to 200 nm and lengths up to 1 μm, with flat tops due to the slow decomposition of $Zn(NH_3)_4^{2+}$ to $Zn(OH)_4^{2-}$ stunting the crystal growth rates, before dehydration to ZnO. Exposure to hydroxide ions causes erosion of the nanorods, resulting in nanotubes and splits on the side planes. Studies involving various pulse energy levels and total irradiation energy at 1 kHz and 250 kHz repetition rates show that there exists the critical threshold pulse energy to induce heterogeneous nucleation favourable for growth into well-defined and individually separated nanowires. Furthermore, studies involving pH variation indicate that ZnO nucleus produced through different reaction pathways according to the pH value of the precursor solution. The size of the obtained hexagonal ZnO nanorods is variable according to the pH of the precursor solution. The ZnO nanorods and nanowires exhibit a broad UV emission peaking at 385 nm, with green emission due to defect states.

4. Acknowledgment

The authors would like to thank Jianrong Qiu from Zhejiang University and Peter G. Kazansky from University of Southampton for helpful discussions. This research is partially supported by Grant-in-Aid for Scientific Research (B), Nippon Sheet Glass Foundation for Materials Science and Engineering (NSG Foundation), and MURATA Science Foundation and Engineering.

5. References

Alivisatos, A. P. (1996). Semiconductor Clusters, Nanocrystals, and Quantum Dots. *Science*, Vol.271, No.5251, (February 1996), pp. 933-937, ISSN 0036-8075

Anker, J. N.; Hall, W. P.; Lyandres, O.; Shah, N. C.; Zhao, J.; Van Duyne, R. P. (2008). Biosensing with plasmonic nanosensors. *Nature Materials*, Vol.7, No.6, (June 2008), pp. 442-453, ISSN 1476-1122

Arnold, M. S.; Avouris,P.; Pan, Z. W. & Wang, Z. L. (2003). Field-Effect Transistors Based on Single Semiconducting Oxide Nanobelts. *Journal of Physical Chemistry B*, Vol.107, No.3, (December 2003), pp. 659-663, ISSN 1520-6106

Baldacchini, T.; Carey, J. E.; Zhou, M. & Mazur, E. (2006). Superhydrophobic Surfaces Prepared by Microstructuring of Silicon Using a Femtosecond Laser. *Langmuir*, Vol.22, No.11, (April 2006), pp. 4917-4919, ISSN 0743-7463

Baruah, S. & Dutta, J. (2009). Hydrothermal growth of ZnO nanostructures. *Science and Technology of Advanced Materials*, Vol.10, No.1, (March 2009), pp. 013001-1-18, ISSN 1468-6996

Braun, A.; Korn, G.; Liu, X.; Du, D.; Squier, J. & Mourou, G. (1995). Self-channeling of high-peak-power femtosecond laser pulses in air. *Optics letters*, Vol.20, No.1, (January 1995), pp. 73-75, ISSN 0146-9592

Cavanagh, R. R.; King, D. S.; Stephenson, J. C. & Heinz, T. F. (1993). Dynamics of nonthermal reactions: femtosecond surface chemistry. *Journal of Physical Chemistry*, Vol.97, No.4, (January 1993), pp. 786-798, ISSN 0022-3654

Chang, G.; Shimotsuma, Y.; Sakakura, M.; Yuasa, T.; Homma, H.; Oyama, M.; Miura, K.; Qiu, J.; Kazansky, P. G. & Hirao, K. (2008). Photo-conversion and evolution of one-dimensional Cu nanoparticles under femtosecond laser irradiation. *Applied surface science*, Vol.254, No.16, (June 2008), pp. 4992-4998 ISSN 0169-4332

Chartier, A. & Bialkowski, S. E. (1997). Photothermal lens spectrometry of homogeneous fluids with incoherent white-light excitation using a cylindrical sample cell. *Optical Engineering*, Vol.36, No.2, (February 1997), pp. 303-311, ISSN 0091-3286

Chen, Z. -Z.; Shi, E. -W.; Zheng, Y. -Q.; Li, W. -J.; Xiao, B. & Zhuang, J. -Y. (2003). Growth of hex-pod-like Cu_2O whisker under hydrothermal conditions. *Journal of Crystal Growth*, Vol.249, No.1-2, (February 2003), pp. 294-300, ISSN 0022-0248

Corkum, P. B.; Rolland, C. & Srinivasan-Rao, T. (1986). Supercontinuum generation in gases. *Physical Review Letters*, Vol.57, No.18, (November 1986), pp. 2268–2271, ISSN 0031-9007

Desvaux, C.; Amiens, C.; Fejes, P.; Renaud, P.; Respaud, M.; Lecante, P.; Snoeck, E. & Chaudret, B. (2005). Multimillimetre-large superlattices of air-stable iron–cobalt nanoparticles. *Nature Materials*, Vol.4, No.10, (October 2005), pp. 750-753, ISSN 1476-1122

Elghanian, R.; Storhoff, J. J.; Mucic, R. C.; Letsinger, R. L. & Mirkin, C. A. (1997). Selective Colorimetric Detection of Polynucleotides Based on the Distance-Dependent

Optical Properties of Gold Nanoparticles. *Science*, Vol.277, No.5329, (August 1997) pp.1078-1081, ISSN 0036-8075

Fan, H. J.; Fuhrmann, B.; Scholz, R.; Syrowatka, F.; Dadgar, A.; Krost, A. & Zacharias, M. (2006). Well-ordered ZnO nanowire arrays on GaN substrate fabricated via nanosphere lithography. *Journal of Crystal Growth*, Vol.287, No.1, (November 2006), pp. 34-38, ISSN 0022-0248

Ferry, V. E.; Sweatlock, L. A.; Pacifici, D. & Atwater, H. A. (2008). Plasmonic Nanostructure Design for Efficient Light Coupling into Solar Cells. *Nano Letters*, Vol.8, No.12, (December 2008), pp. 4391-4397, ISSN 1530-6984

Feurer, T.; Theobald, W.; Sauerbrey, R.; Uschmann, I.; Altenbernd, D.; Teubner, U.; Gibbon, P.; Förster, E.; Malka, G.; Miquel, J. L. (1997). Onset of diffuse reflectivity and fast electron flux inhibition in 528-nm-laser–solid interactions at ultrahigh intensity. *Physical Review E*, Vol.56, No.4, (October 1997), pp. 4608-4614, ISSN 1063-651X

Fratesi, R. & Roventi, G. (1992). Electrodeposition of zinc-nickel alloy coatings from a chloride bath containing NH_4Cl. *Journal of Applied Electrochemistry*, Vol.22, No.7, (July 1992), pp. 657-662, ISSN 0021-891X

Gates, B.; Mayers, B.; Grossman, A. & Xia, Y. (2002). A Sonochemical Approach to the Synthesis of Crystalline Selenium Nanowires in Solutions and on Solid Supports. *Advanced Materials*, Vol.14, No.23, (December 2002), pp. 1749-1752, ISSN 0935-9648

Goux, A.; Pauporté, T.; Chivot, J. & Lincot, D. (2005). Temperature effects on ZnO electrodeposition. *Electrochimica Acta*, Vol.50, No.11, (April 2005), pp. 2239-2248, ISSN 0013-4686

Hatanaka, K.; Miura, T. & Fukumura, H. (2004). White X-ray pulse emission of alkali halide aqueous solutions irradiated by focused femtosecond laser pulses: a spectroscopic study on electron temperatures as functions of laser intensity, solute concentration, and solute atomic number. *Chemical Physics*, Vol.299, No.2-3, (April 2004), pp. 265-270, ISSN 0301-0104

Heo, Y. W.; Varadarajan, V.; Kaufman, M.; Kim, K.; Norton, D. P.; Ren, F. & Fleming, P. H. (2002). Site-specific growth of ZnO nanorods using catalysis-driven molecular-beam epitaxy. *Applied Physics Letters*, Vol.81, No.16, (August 2002), pp. 3046-3048, ISSN 0003-6951

Hosono, E.; Fujihara, S.; Honma, I. & Zhou, H. (2005). The Fabrication of an Upright-Standing Zinc Oxide Nanosheet for Use in Dye-Sensitized Solar Cells. *Advanced Materials*, Vol.17, No.17, (July 2005), pp. 2091-2094, ISSN 0935-9648

Hu, J. T.; Odom, T. W. & Lieber, C. M. (1999). Chemistry and Physics in One Dimension: Synthesis and Properties of Nanowires and Nanotubes. *Accounts of Chemical Research*, Vol.32, No.5, (February 1999), pp. 435-445, ISSN 0001-4842

Huang, M. H.; Mao, S.; Feick, H.; Yan, H.; Wu, Y.; Kind, H.; Weber, E.; Russo, R. & Yang, P. (2001a). Room-Temperature Ultraviolet Nanowire Nanolasers. *Science*, Vol.292, No.5523, (June 2001), pp. 1897-1899, ISSN 0036-8075

Huang, M. H.; Wu, Y.; Feick, H.; Tran, N.; Weber, E. & Yang, P. (2001b). Catalytic Growth of Zinc Oxide Nanowires by Vapor Transport. *Advanced Materials*, Vol.13, No.2, (January 2001), pp. 113-116, ISSN 0935-9648

Hubert, B.; Naghavi, N.; Canava, B.; Etcheberry, A. & Lincot, D. (2007). Thermodynamic and experimental study of chemical bath deposition of Zn(S,O,OH) buffer layers in basic aqueous ammonia solutions. Cell results with electrodeposited $CuIn(S,Se)_2$ absorbers. *Thin Solid Films*, Vol.515, No.15, (May 2007), pp. 6032-6035, ISSN 0040-6090

Jia, T. Q.; Zhao, F. L.; Huang, M.; Chen, H. X.; Qiu, J. R.; Li, R. X.; Xu, Z. Z. & Kuroda, H. (2006a). Alignment of nanoparticles formed on the surface of 6H-SiC crystals

irradiated by two collinear femtosecond laser beams. *Applied Physics Letters*, Vol.88, No.11, (March 2006), pp. 111117-1-3, ISSN 0003-6951

Jia, T. Q.; Chen, H. X.; Huang, M.; Wu, X. J.; Zhao, F. L.; Baba, M.; Suzuki, M.; Kuroda, H.; Qiu, J. R.; Li, R. X. & Xu, Z. Z. (2006b). ZnSe nanowires grown on the crystal surface by femtosecond laser ablation in air. *Applied Physics Letters*, Vol.89, No.10, (September 2006), pp. 101116-1-3, ISSN 0003-6951

Jin, R.; Cao, Y. W.; Mirkin, C. A.; Kelly, K. L.; Schatz, G. C. & Zheng, J. G. (2001). Photoinduced Conversion of Silver Nanospheres to Nanoprisms. *Science*, Vol.294, No.5548, (November 2001), pp. 1901-1903, ISSN 0036-8075

Kabashin, A. V.; Meunier, M.; Kingston, C. & Luong, J. H. T. (2003). Fabrication and Characterization of Gold Nanoparticles by Femtosecond Laser Ablation in an Aqueous Solution of Cyclodextrins. *Journal of Physical Chemistry B*, Vol.107, No.19, (April 2003), pp. 4527-4531, ISSN 1520-6106

Kanehira, S.; Si., J.; Qiu, J.; Fujita, K. & Hirao, K. (2005). Periodic Nanovoid Structures via Femtosecond Laser Irradiation. *Nano Letters*, Vol.5, No.8, (August 2005), pp. 1591-1595, ISSN 1530-6984

Kar, S.; Dev, A. & Chaudhuri, S. (2006). Simple Solvothermal Route To Synthesize ZnO Nanosheets, Nanonails, and Well-Aligned Nanorod Arrays. *Journal of Physical Chemistry B*, Vol.110, No.36, (August 2006), pp. 17848-17853, ISSN 1520-6106

Kawai, J.; Nakajima, K. & Gohshi, Y. (1993). Copper Lβ/Lα X-ray emission intensity ratio of copper compounds and alloys. *Spectrochimica Acta Part B: Atomic Spectroscopy*, Vol.48, No.10, (August 1993), pp. 1281-1290, ISSN 0584-8547

Kawasaki, M. & Masuda, K. (2005). Laser Fragmentation of Water-Suspended Gold Flakes via Spherical Submicroparticles to Fine Nanoparticles. *Journal of Physical Chemistry B*, Vol.109, No.19, (April 2005), pp. 9379-9388, ISSN 1520-6106

Kong, X. Y. & Wang, Z. L. (2003). Spontaneous Polarization-Induced Nanohelixes, Nanosprings, and Nanorings of Piezoelectric Nanobelts. *Nano Letters*, Vol.3, No.12, (August 2003), pp. 1625-1631, ISSN 1530-6984

Kong, Y. C.; Yu, D. P.; Zhang, B.; Fang, W. & Feng, S. Q. (2001). Ultraviolet-emitting ZnO nanowires synthesized by a physical vapor deposition approach. *Applied Physics Letters*, Vol.78, No.4, (January 2001), pp. 407-409, ISSN 0003-6951

Kupersztych, J.; Raynaud, M. & Riconda, C. (2004). Electron acceleration by surface plasma waves in the interaction between femtosecond laser pulses and sharp-edged overdense plasmas. *Physics of Plasmas*, Vol.11, No.4, (April 2004), pp. 1669-1673, ISSN 1070-664X

Le, H. Q.; Chua, S. J.; Koh, Y. W.; Loh, K. P.; Chen, Z.; Thompson, C. V. & Fitzgerald, E. A. (2005). Growth of single crystal ZnO nanorods on GaN using an aqueous solution method. *Applied Physics Letters*, Vol.87, No.10, (September 2005), pp. 101908-1-3, ISSN 0003-6951

Lee, C. J.; Lee, T. J.; Lyu, S. C.; Zhang, Y.; Ruh, H. & Lee, H. J. (2002). Field emission from well-aligned zinc oxide nanowires grown at low temperature. *Applied Physics Letters*, Vol.81, No.19, (September 2002), pp. 3648-3650, ISSN 0003-6951

Lee, E. T. Y.; Shimotsuma, Y.; Sakakura, M.; Nishi, M.; Miura, K. & Hirao, K. (2008). Photo-initiated growth of zinc oxide (ZnO) nanorods. *Materials Letters*, Vol.62, No.24, (September 2008), pp. 4044-4046, ISSN 0167-577X

Lee, E. T. Y.; Shimotsuma, Y.; Sakakura, M.; Nishi, M.; Miura, K. & Hirao, K. (2009). Ultrashort Pulse Manipulation of ZnO Nanowire Growth. *Journal of Nanoscience and Nanotechnology*, Vol.9, No.1, (January 2009), pp. 618-626, ISSN 2078-0338

Li, W.; Shi, E.; Zhong, W.; Yin, Z. (1999). Growth mechanism and growth habit of oxide crystals. *Journal of Crystal Growth*, Vol.203, No.1-2, (May 1999), pp. 186-196, ISSN 0022-0248

Lieber, C. M. (1998). One-dimensional nanostructures: Chemistry, physics & applications. *Solid State Communications*, Vol.107, No.11, (August 1998), pp. 607-616, ISSN 0038-1098

Lin, P. -F.; Ko, C. -Y.; Lin, W. -T. & Lee, C. T. (2007). Effects of processing parameters on ultraviolet emission of In-doped ZnO nanodisks grown by carbothermal reduction. *Materials Letters*, Vol.61, No.8-9, (April 2007), pp. 1767-1770, ISSN 0167-577X

Lin, Y. -S.; Wu, S. -H.; Hung, Y.; Chou, Y. -H.; Chang, C.; Lin, M. -L.; Tsai, C. -P. & Mou, C. -Y. (2006). Multifunctional Composite Nanoparticles: Magnetic, Luminescent, and Mesoporous. *Chemistry of Materials*, Vol.18, No.22, (October 2006), pp. 5170-5172, ISSN 0897-4756

Lin, Z.; Zhigilei, L. V. & Celli, V. (2008). Electron-phonon coupling and electron heat capacity of metals under conditions of strong electron-phonon nonequilibrium. *Physical Review B*, Vol.77, No.7, (February 2008), pp. 075133-1-17, ISSN 0163-1829

Link, S.; Burda, C.; Mohamed, M. B.; Nikoobakht, B. & El-Sayed, M. A. (1999). Laser Photothermal Melting and Fragmentation of Gold Nanorods: Energy and Laser Pulse-Width Dependence. *Journal of Physical Chemistry A*, Vol.103, No.9, (March 1999), pp. 1165-1170, ISSN 1089-5639

Link, S.; Burda, C.; Mohamed, M. B.; Nikoobakht, B. & El-Sayed, M. A. (2000). Femtosecond transient-absorption dynamics of colloidal gold nanorods: Shape independence of the electron-phonon relaxation time. *Physical Review B*, Vol.61, No.9, (March 2000), pp. 6086-6090, ISSN 0163-1829

Lipinska-Kalita, K. E.; Krol, D. M.; Hemley, R. J.; Mariotto, G.; Kalita, P. E. & Ohki, Y. (2005). Synthesis and characterization of metal-dielectric composites with copper nanoparticles embedded in a glass matrix: A multitechnique approach. *Journal of Applied Physics*, Vol.98, No.5, (September 2005), pp. 054301-1-6, ISSN 0021-8979

Liu, S. -D.; Cheng, M. -T.; Yang, Z. -J. & Wang, Q. -Q. (2008). Surface plasmon propagation in a pair of metal nanowires coupled to a nanosized optical emitter. *Optics Letters*, Vol.33, No.8, (April 2008), pp. 851-853, ISSN 0146-9592

Liu, W.; Kosareva, O.; Golubtsov, I. S.; Iwasaki, A.; Becker, A.; Kandidov, V. P. & Chin, S. L. (2002). Random deflection of the white light beam during self-focusing and filamentation of a femtosecond laser pulse in water. *Applied Physics B: Lasers and Optics*, Vol.75, No.4-5, (October 2002), pp. 595–599, ISSN 0946-2171

Lu, A. -H.; Schmidt, W.; Matoussevitch, N.; Bönnemann, H.; Spliethoff, B.; Tesche, B.; Bill, E.; Kiefer, W. & Schüth, F. (2004). Nanoengineering of a Magnetically Separable Hydrogenation Catalyst. *Angewandte Chemie International Edition*, Vol.43, No.33, (August 2004), pp. 4303-4306, ISSN 1433-7851

Macchi, A.; Cornolti, F.; Pegoraro, F.; Liseikina, T. V.; Ruhl, H. & Vshivkov, V. A. (2001). Surface Oscillations in Overdense Plasmas Irradiated by Ultrashort Laser Pulses. *Physical Review Letters*, Vol.87, No.20, (October 2001), pp. 205004-1-4, ISSN 0031-9007

Maier, S. A.; Kik, P. G.; Atwater, H. A.; Meltzer, S.; Harel, E.; Koel, B. E. & Requicha, A. A. G. (2003). Local detection of electromagnetic energy transport below the diffraction limit in metal nanoparticle plasmon waveguides. *Nature Materials*, Vol.2, No.4, (April 2003), pp. 229-232, ISSN 1476-1122

Morales, A. M. & Lieber, C. M. (2008). A Laser Ablation Method for the Synthesis of Crystalline Semiconductor Nanowires. *Science*, Vol.279, No.5348, (January 1998), pp. 208-211, ISSN 0036-8075

Muskens, O. L.; Fatti, N. D. & Vallee, F. (2006). Femtosecond Response of a Single Metal Nanoparticle. *Nano Letters*, Vol.6, No.3, (January 2006), pp. 552-556, ISSN 1530-6984

Nakao, A.; Shimotsuma, Y.; Nishi, M.; Miura, K. & Hirao, K. (2008). Morphological control of nanoparticles by femtosecond laser irradiation. *Journal of Ceramic Processing Research*, Vol.9, No.4, (August 2008) pp. 425-429, ISSN 1229-9162

Ohta, H. & Hosono, H. (2004). Transparent oxide optoelectronics. *Materials Today*, Vol.7, No.6, (June 2004), pp. 42-51, ISSN 1369-7021

Pacholski, C.; Kornowski, A. & Weller, H. (2002). Self-Assembly of ZnO: From Nanodots to Nanorods. *Angewandte Chemie International Edition*, Vol.41, No.7, (April 2002), pp. 1188-1191, ISSN 1433-7851

Pan, Z. W.; Dai, Z. R. & Wang, Z. L. (2001). Nanobelts of Semiconducting Oxides. *Science*, Vol.291, No.5510, (March 2001), pp. 1947-1949, ISSN 0036-8075

Park, W. I.; Kim, D. H.; Jung, S.-W. & Yi, G. -C. (2002). Metalorganic vapor-phase epitaxial growth of vertically well-aligned ZnO nanorods. *Applied Physics Letters*, Vol.80, No.22, (April 2002), pp. 4232-4234, ISSN 0003-6951

Peulon, S. & Lincot, D. (1998). Mechanistic Study of Cathodic Electrodeposition of Zinc Oxide and Zinc Hydroxychloride Films from Oxygenated Aqueous Zinc Chloride Solutions. *Journal of the Electrochemical Society*, Vol.145, No.3, (March 1998), pp. 864-874, ISSN 0013-4651

Podlipensky, A.; Lange, J.; Seifert, G.; Graener, H. & Cravetchi, I. (2003). Second-harmonic generation from ellipsoidal silver nanoparticles embedded in silica glass. *Optics Letters*, Vol.28, No.9, (May 2003) pp. 716-718, ISSN 0146-9592

Qiu, J.; Jiang, X.; Zhu, C.; Shirai, M.; Si, J.; Jiang, N. & Hirao, K. (2004). Manipulation of Gold Nanoparticles inside Transparent Materials. *Angewandte Chemie International Edition*, Vol.43, No.17, (April 2004), pp. 2230-2234, ISSN 1433-7851

Rao, A. M.; Eklund, P. C.; Bandow, S.; Thess, A. & Smalley, R. E. (1997). Evidence for charge transfer in doped carbon nanotube bundles from Raman scattering. *Nature*, Vol.388, No.6639, (July 1997), pp. 255-259, ISSN 0028-0836

Sauer, G.; Brehm, G.; Schneider, S.; Nielsch, K.; Choi, J.; Göring, P.; Gösele, U.; Miclea, P. & Wehrspohn, R. B. (2006). Surface-enhanced Raman spectroscopy employing monodisperse nickel nanowire arrays. *Applied Physics Letters*, Vol.88, No.2, (January 2006), pp. 023106-1-3, ISSN 0003-6951

Sberveglieri, G.; Baratto, C.; Comini, E.; Faglia, G.; Ferroni, M.; Ponzoni, A. & Vomiero, A. (2007). Synthesis and characterization of semiconducting nanowires for gas sensing. *Sensors and Actuators B*, Vol.121, No.1, (January 2007) pp. 208-213, ISSN 0925-4005

Shen, M. Y.; Crouch, C. H.; Carey, J. E. & Mazur, E. (2004). Femtosecond laser-induced formation of submicrometer spikes on silicon in water. *Applied Physics Letters*, Vol.85, No.23, (September 2004), pp. 5694-5696 ISSN 0003-6951

Shimotsuma, Y.; Kazansky, P. G.; Qiu, J.; Hirao, K. (2003). Self-Organized Nanogratings in Glass Irradiated by Ultrashort Light Pulses. *Physical Review Letters*, Vol.91, No.24, (December 2003), pp. 247405-1-4, ISSN 0031-9007

Shimotsuma, Y.; Sakakura, M.; Miura, K.; Qiu, J.; Kazansky, P. G.; Fujita, K. & Hirao, K. (2007). Application of Femtosecond-Laser Induced Nanostructures in Optical Memory. *Journal of Nanoscience and Nanotechnology*, Vol.7, No.1, (January 2007), pp. 94-104, ISSN 2078-0338

Shimotsuma, Y.; Yuasa, T.; Homma, H.; Sakakura, M.; Nakao, A.; Miura, K.; Hirao, K.; Kawasaki, M.; Qiu, J. & Kazansky, P. G. (2007). Photoconversion of Copper Flakes

to Nanowires with Ultrashort Pulse Laser Irradiation. *Chemistry of Materials*, Vol.19, No.6, (February 2007), pp. 1206-1208, ISSN 0897-4756

Stalmashonak, A.; Podlipensky, A.; Seifert, G. & Graener, H. (2009). Intensity-driven, laser induced transformation of Ag nanospheres to anisotropic shapes. *Applied Physics B: Lasers and Optics*, Vol.94, No.3, (November 2009), pp. 459-465, ISSN 0946-2171

Stuart, B. C.; Feit, M. D.; Herman, S.; Rubenchik, A. M.; Shore, B. W. & Perry, M. D. (1995). Laser-Induced Damage in Dielectrics with Nanosecond to Subpicosecond Pulses. *Physical Review Letters*, Vol.74, No.12, (March 1995) pp. 2248-2251, ISSN 0031-9007

Sylvestre, J. -P.; Kabashin, A. V.; Sacher, E.; Meunier, M. & Luong, J. H. T. (2004). Stabilization and Size Control of Gold Nanoparticles during Laser Ablation in Aqueous Cyclodextrins. *Journal of the American Chemical Society*, Vol.126, No.23, (May 2004), pp. 7176-7177, ISSN 0002-7863

Tamaki, Y.; Asahi, T. & Masuhara, H. (2002). Nanoparticle Formation of Vanadyl Phthalocyanine by Laser Ablation of Its Crystalline Powder in a Poor Solvent. *Journal of Physical Chemistry A*, Vol.106, No.10, (January 2002), pp. 2135-2139, ISSN 1089-5639

Tilaki, R. M.; Iraji-zad, A. & Mahdavi, S. M. (2007). Size, composition and optical properties of copper nanoparticles prepared by laser ablation in liquids. *Applied Physics A: Materials Science & Processing*, Vol.88, No.2, (May 2007), pp. 415-419, ISSN 0947-8396

Tull, B. R.; Carey, J. E.; Sheehy, M. A.; Friend, C. & Mazur, E. (2006). Formation of silicon nanoparticles and web-like aggregates by femtosecond laser ablation in a background gas. *Applied Physics A: Materials Science & Processing*, Vol.83, No.3, (June 2006), pp. 341-346, ISSN 0947-8396

Tzortzakis, S.; Sudrie, L.; Franco, M.; Prade, B.; Mysyrowicz, A.; Couairon, A. & Berge, L. (2001). Self-Guided Propagation of Ultrashort IR Laser Pulses in Fused Silica. *Physical Review Letters*, Vol.87, No.21, (November 2001), pp. 213902-1-4, ISSN 0031-9007

Unal, A. A.; Stalmashonak, A.; Seifert, G.; Graener, H. (2009). Ultrafast dynamics of silver nanoparticle shape transformation studied by femtosecond pulse-pair irradiation. *Physical Review B*, Vol.79, No.11, (March 2009), pp. 115411-1-7, ISSN 1098-0121

Vanheusden, K.; Warren, W. L.; Seager, C. H.; Tallant, D. R.; Voigt, J. A. & Gnade, B. E. (1996). Mechanisms behind green photoluminescence in ZnO phosphor powders. *Journal of Applied Physics*, Vol.79, No.10, (February 1996), pp. 7983-7990, ISSN 0021-8979

Vogel, A.; Noack, J.; Hüttman, G. & Paltauf, G. (2005). Mechanisms of femtosecond laser nanosurgery of cells and tissues. *Applied Physics B: Lasers and Optics*, Vol.81, No.8, (November 2005), pp. 1015-1047, ISSN 0946-2171

Wagner, R. S. & Ellis, W. C. (1964). Vapr-Liquid-Solid Mechanism of Single Crystal Growth. *Applied Physics Letters*, Vol.4, No.5, (February 1964), pp. 89-90, ISSN 0003-6951

Wu, N.; Shimotsuma, Y.; Nishi, M.; Sakakura, M.; Miura, K. & Hirao, K. (2010). Photo-initiation of ZnO nanorod formation by femtosecond laser irradiation. *Journal of the Ceramic Society of Japan*, Vol.118, No.1374, (February 2010), pp. 147-151 ISSN 1882-0743

Xiang, Y.; Wu, X.; Liu, D.; Jiang, X.; Chu, W.; Li, Z.; Ma, Y.; Zhou, W. & Xie, S. (2006). Formation of Rectangularly Shaped Pd/Au Bimetallic Nanorods: Evidence for Competing Growth of the Pd Shell between the {110} and {100} Side Facets of Au Nanorods. *Nano Letters*, Vol.6, No.10, (September 2006), pp. 2290-2294, ISSN 1530-6984

Yamabi, S. & Imai, H. (2002). Growth conditions for wurtzite zinc oxide films in aqueous solutions. *Journal of Materials Chemistry*, Vol.12, No.12, (September 2002), pp. 3773-3778, ISSN 0959-9428

Yang, M.; Pang, G.; Jiang, L. & Feng, S. (2006). Hydrothermal synthesis of one-dimensional zinc oxides with different precursors. *Nanotechnology*, Vol.17, No.1, (January 2006), pp. 206-212, ISSN 0957-4484

Yim, S. -Y.; Ahn, H. -G.; Je, K. -C.; Choi, M.; Park, C. W.; Ju, H. & Park, S. -H. (2007). Observation of red-shifted strong surface plasmon scattering in single Cu nanowires. *Optics Express*, Vol.15, No.16, (August 2007), pp. 10282-10287, ISSN 1094-4087

Yu, K.; Jin, Z.; Liu, X.; Zhao, J. & Feng, J. (2007). Shape alterations of ZnO nanocrystal arrays fabricated from $NH_3 \cdot H_2O$ solutions. *Applied Surface Science*, Vol.253, No.8, (October 2007), pp. 4072-4078, ISSN 0169-4332

Zepf, M.; Tsakiris, G. D.; Pretzler, G.; Watts, I.; Chambers, D. M.; Norreys, P. A.; Andiel, U.; Dangor, A. E.; Eidmann, K.; Gahn, C.; Machacek, A.; Wark, J. S. & Witte, K. (1998). Role of the plasma scale length in the harmonic generation from solid targets. *Physical Review E*, Vol.58, No.5, (November 1998), pp. R5253-R5256, ISSN 1063-651X

Zhang, F.; Wang, X.; Ai, S.; Sun, Z.; Wan, Q.; Zhu, Z.; Xian, Y.; Jin, L. & Yamamoto, K. (2004). Immobilization of uricase on ZnO nanorods for a reagentless uric acid biosensor. *Analytica Chimica Acta*, Vol.519, No.2, (August 2004), pp. 155-160, ISSN 0003-2670

Zhang, H.; Yang, D.; Ma, X.; Ji, Y.; Xu, J. & Que, D. (2004). Synthesis of flower-like ZnO nanostructures by an organic-free hydrothermal process. *Nanotechnology*, Vol.15, No.5, (May 2004), pp. 622-626, ISSN 0957-4484

Zhang, J.; Sun, L.; Liao, C. & Yan, C. (2002a). A simple route towards tubular ZnO. *Chemical Communications*, Vol.2002, No.3, (January 2002), pp. 262-263, ISSN 1359-7345

Zhang, J.; Sun, L. D.; Yin, J. L.; Su, H. L.; Liao, C. S. & Yan, C. H. (2002b). Control of ZnO Morphology via a Simple Solution Route. *Chemistry of Materials*, Vol.14, No.10, (September 2002), pp. 4172-4177, ISSN 0897-4756

Zhang, X. Y.; Dai, J. Y.; Ong, H. C.; Wang, N.; Chan, H. L. W. & Choy, C. L. (2004). Hydrothermal synthesis of oriented ZnO nanobelts and their temperature dependent photoluminescence. *Chemical Physics Letters*, Vol.393, No.1-3, (July 2004), pp. 17-21, ISSN 0009-2614

Zhang, Y. & Mu, J. (2007). Controllable synthesis of flower- and rod-like ZnO nanostructures by simply tuning the ratio of sodium hydroxide to zinc acetate. *Nanotechnology*, Vol.18, No.7, (February 2007), pp. 075606-1-6, ISSN 0957-4484

Zhang, Y.; Russo, R. E. & Mao, S. S. (2005). Femtosecond laser assisted growth of ZnO nanowires. *Applied Physics Letters*, Vol.87, No.13, (September 2005), pp. 133115-1-3, ISSN 0003-6951

Zhang, Y.; Suenaga, K.; Colliex, C. & Iijima, S. (1998). Coaxial Nanocable: Silicon Carbide and Silicon Oxide Sheathed with Boron Nitride and Carbon. *Science*, Vol.281, No.5379, (August 1998), pp. 973-975, ISSN 0036-8075

Nanowires - Fundamental Research

Edited by Dr. Abbass Hashim

ISBN 978-953-307-327-9
Hard cover, 552 pages
Publisher InTech
Published online 19, July, 2011
Published in print edition July, 2011

Understanding and building up the foundation of nanowire concept is a high requirement and a bridge to new technologies. Any attempt in such direction is considered as one step forward in the challenge of advanced nanotechnology. In the last few years, InTech scientific publisher has been taking the initiative of helping worldwide scientists to share and improve the methods and the nanowire technology. This book is one of InTechâ€™s attempts to contribute to the promotion of this technology.

How to reference

In order to correctly reference this scholarly work, feel free to copy and paste the following:

Kiyotaka Miura, Kazuyuki Hirao and Yasuhiko Shimotsuma (2011). Nanowire formation under femtosecond laser radiation in liquid, Nanowires - Fundamental Research, Dr. Abbass Hashim (Ed.), ISBN: 978-953-307-327-9, InTech, Available from: http://www.intechopen.com/books/nanowires-fundamental-research/nanowire-formation-under-femtosecond-laser-radiation-in-liquid

INTECH
open science | open minds

InTech Europe
University Campus STeP Ri
Slavka Krautzeka 83/A
51000 Rijeka, Croatia
Phone: +385 (51) 770 447
Fax: +385 (51) 686 166
www.intechopen.com

InTech China
Unit 405, Office Block, Hotel Equatorial Shanghai
No.65, Yan An Road (West), Shanghai, 200040, China
中国上海市延安西路65号上海国际贵都大饭店办公楼405单元
Phone: +86-21-62489820
Fax: +86-21-62489821

IntechOpen